

Abstract

Photovoltaic system generates electricity by the direct conversion of the sun's energy and it is a modular system because it is built out of several pieces of elements. The theoretical studies of PV and modeling techniques using equivalent electric circuits carried out and the characteristics of PV cell have been investigated. The new model of PV implemented in pspice program, the optimum voltage was (17volt) and optimum current was (4.41Ampere).

This model is used in the DC-DC converter which has the following characteristics, the variable output voltage is (1.5V-12V), switching frequency (20 kHz), duty cycle (0.1- 0.7) and the output power (1W-41.6W), the system has been design and tested by pspice program. The application of PV and battery implement in the DC-DC converter, the results of the converter simulation obtained from both two input show a good agreement.

Acknowledgment

Praise is to Allah lord of the creation. Best prayer and peace be unto, the prophet Muhammad messenger of Allah, and his pure holy descendants, and Nobel companions.

Then, I would like to express my gratitude to my supervisors Dr. Zainab M. Kubba and for her valuable guidance and constant help through the course of this work.

My personal thank to the University president, the dean of the College of Science and the Head of Physics Department Dr. Ahmad Kamal Ahmad and the Staff of Physics Department at Nahrain University for providing the opportunity and financial support to accomplish this study.

I would like to thank my friends Ahmed Shakir Mahmood and Omar Ayad Jalal for their assistance, and for being with me all through the course of my research.

My deep gratitude to my family who were very patient and encouraging during the period of my study.

Zaid

15 / 4 /2008

APPENDIX A
DATA SHEET

APPENDIX B
DATA SHEET



جمهورية العراق
وزارة التعليم العالي و البحث العلمي
جامعة النهرين
كلية العلوم
قسم الفيزياء

التحليل وتطبيق بواسطة الحاسبة للخلية الكهروضوئية في المغير المستمر

رسالة

مقدمة إلى كلية العلوم في جامعة النهرين وهي جزء من متطلبات نيل

درجة الماجستير في

الفيزياء

من قبل

زيد سمير جبار السامرائي

(بكالوريوس ١٩٩٨)

بإشراف

الدكتورة زينب منذر يونس كبة

في

نيسان ٢٠٠٨ م

ربيع الثاني ١٤٢٩ هـ

Certification

I certify that this thesis entitled “*A Computer simulation and application of PV cell on DC-DC converter*” is prepared by *Mr. Zaid Samir Jabbar Al-Samarai* under my supervision at the College of Science of Nahrain University in partial fulfillment of the requirements for the degree of **Master of Science in Physics**.

Supervisor: Dr. Zainab M. Kubba

Date: / /2008

In view of the recommendations, I present this thesis for debate by the examination committee.

Dr. Ahmad K. Ahmad

Title: Assistant Professor

Head of Physics Department

Date: / /2008

Contents

	Acknowledgment	I
	Abstract	II
	List of symbols & abbreviations	III
	List of table	V
	List of figures	VI
Chapter One	Introduction	1-7
1-1	Introduction	1
1-2	The Photovoltaic System	2
1-3	Solar cells	3
1-4	DC-DC Converters	4
1-5	Multiple-Input DC-DC Converters	4
1-6	Pspice	4
1-7	Literature Survey	5
1-8	Thesis Overviews	6
1-9	The aim of thesis	7
Chapter Two	Fundamental of Characteristics of the PV & Converters	8-21
2-1	Introduction	8
2-2	P-N Junction	8
2-2-1	P-N Junction Characteristics	11
2-3	The P-N Junction PV Cell	12
2-3-1	Photovoltaic Modeling	14
2-3-2	The Fundamental Electric Parameters of the PV Cell	14
2-3-3	The dark & illuminated $I - V$ characteristics	17
2-4	PV Modules	20
2-5	Step-Down (Buck) Converter	21
2-5-1	Continuous-Conduction Mode	23
2-5-2	Boundary between Continuous and Discontinuous Conduction	25
2-5-3	Discontinuous-Conduction Mode	26
2-5-4	Output Voltage Ripple	29
2-6	Output Control Circuit	30
2-7	A multiple Input DC-DC Converter	31

Chapter Three	PV Panel Simulation Results	33-52
3-1	Introduction	33
3-2	Panel Parameters Calculation	33
3-3	Simulation of the PV panel	34
3-4	Simulation Results	39
3-5	Hierarchical Block	48
Chapter Four	Testing the PV Panel Model in Converter Circuit	53-69
4-1	Introduction	53
4-2	Converter Circuit Design	53
4-2-1	PWM Generator	55
4-2-2	MOSFET Gate Drive Circuit	57
4-2-3	Sources Control Circuit	57
4-3	The System Configuration	58
4-4	Two input buck converter simulation results	58
Chapter Five	Conclusions and future work	70-71
5-1	Conclusions	70
5-2	Future work	70
References		72-73
Appendix A		
Appendix B		

Republic of Iraq
Ministry of Higher Education and Scientific Research
Nahrain University
College of Science
Physics Department



A Computer Simulation and Application of PV cell on DC-DC Converter

A Thesis

Submitted to the College of Science of Nahrain
University in Partial Fulfillment of the Requirements for
the Degree of

Master of Science

In

Physics

By

Zaid Samir Jabbar Al-Samarai

(B.Sc.1998)

Supervised by

Dr. Zainab M. Kubba

In

Rabia II 1429 A. H.

April 2008 A. D.

Examination Committee Certification

We certify that we have read the thesis entitled "*A Computer Simulation and application of PV cell on DC-DC Converter*" and as an examination committee, examined the student **Mr. Zaid Samir Jabbar** on its contents, and that in our opinion it is adequate for the partial fulfillment of the requirements of the degree of **Master of Science in Physics**.

Signature:

Name: **Dr. Kader H. AL- Shara**

Title: **Assistant Professor**

(**Chairman**)

Date: **/7/2008**

Signature:

Name: **Dr. Safa S. Mahdi**

Title: **Assistant Professor**

(**Member**)

Date: **/7/2008**

Signature:

Name: **Dr. Azhar J. Dawud**

Title: **Lecturer**

(**Member**)

Date: **/7/2008**

Signature:

Name: **Dr. Zainab M. Kubba**

Title: **Lecturer**

(**Supervisor**)

Date: **/7/2008**

Approved by the College Committee of Postgraduate studies

Signature:

Name: **Dr. LAITH ABDUL AZIZ Al- ANI**

Title: **Assistant Professor**

(**Dean of the College of Science**)

Date: **/ /2008**

References

- [1] Denizar Cruz Martins, Rogers Demonti, Ivo Barbi "*Static Conversion System for Treatment of the Solar Energy and Interconnection with the mains power supply*", 5th Brazilian power electronics conference. 1999.
- [2] Luis Castaner, Santiago Silvestre "*Modeling Photovoltaic System using Pspice*", John Wiley & Sons. Inc, September 2002.
- [3] G.N.Tiwari, Sangeeta Suneja "*Solar Thermal Engineering Systems*", Narosa Publishing House, 1997.
- [4] Cederblad Henrik, Fasselund Joar, Nordin Olof "*nCube-Power supply*" Thesis, Narvik University College, June 2003.
- [5] Hirofumi Matsuo, Wenzhong Lin, Fujio Kurokawa, Tetsuro Shigemizu and Nobuya Watanabe " *Characteristics of the Multiple-Input Dc-Dc Converter*", IEEE Transactions on industrial electronics, vol. 51, no. 3, June 2004.
- [6] Mikael Knuuti "*High Speed 2KW Dc-Dc converter*", Thesis, Institution for Computer Science and Electronics Malardalens University, 2007.
- [7] Dave Turcotte, Michael Ross and Farah Sheriff "*Photovoltaic Hybrid System sizing and simulation tools status and needs*", OPJ, November 2001.
- [8] The History of PV, www.corrosion.doctor.org/Solar/photo-hist.htm., 2007
- [9] M.R.Mack, Mie Aust "*Solar power for Telecommunication*", TJA, vol.29, no. 1, 1979.
- [10] Chuck Wright "*Simulating Junior solar sprint with spice*" www.chuck.wright.com/projects.html., 2007
- [11] Greg Waldo "*Pspice Model of the Hubble Space Telescope Electrical Power System*", Greenbelt, Maryland, August 2002.
- [12] Intusoft Newsletter Issue 78, November 2005.

- [13] A.Aziz, K.Kassmi "*Symbolization of the electric diagram of the marketed solar panels in the Orcad-Pspice environment*" M.J. Condensed Mater, vol. 7, no. 1, January 2006.
- [14] Nicholas D. Benavides and Patrick L. Chapman "*Power Budgeting of a Multiple-input Buck-Boost Converter*", IEEE Transactions on power electronics, vol. 20, no. 6, November 2005.
- [15] Tocci "*Electronic Devices*", Charles E. Merrill Publishing, 3rd Edition, 1983.
- [16] Donald A.Neamen "*Semiconductor Physics and devices*", Richard D.Irwin.Inc, 1992.
- [17] G.Beghi "*Performance of Solar Energy Converters: Thermal Collectors and Photovoltaic Cells*", D.Reidel Publishing Company, 1981.
- [18] Mohan "*Power Electronics Converters, Application, and Design*", John Wiley & Sons. Inc, 2nd Edition, 1995.
- [19] Parag Bhide and S.R.Bhat "*Modular Power Conditioning Unit for Photovoltaic Application*", IEEE, 1992.
- [20] Everett Rogers "*Understanding boost power stages in switch mode supplies*", application report, Texas Instruments, 1999.

الخلاصة

المنظومات الكهروضوئية تولد الكهرباء بواسطة التحويل المباشر للطاقة الشمسية وتعتبر نظام متكامل بسبب كونها مركبة من مجموعة قطع من العناصر. الدراسة النظرية للأنظمة الشمسية وتقنيات أنشاء موديل لها باستخدام دوائر كهربائية مكافئة كذلك خصائص الخلية الشمسية ستكون مطروقة في هذا البحث. الموديل الجديد للخلية الشمسية سيتم تحقيقه باستخدام برنامج التحليل pspice. الفولتية المثالية كانت 17volt والتيار المثالي كان 4.41A.

هذا الموديل سيستخدم في المغير المستمر والذي يمتلك المواصفات التالية، فولتية خرج متغير من (1.5V-12V)، التردد المفتاحي 20kHz ، دورة الفرض (0.1-0.7)، وقدرة الخرج من (1W-41.6W). المنظومة مصممة ومفحوصة بواسطة برنامج التحليل pspice. تطبيقات موديل الخلية الشمسية والبطارية ستنفذ في المغير المستمر. نتائج التحليل للمغير التي حصلنا عليها من كلا المدخلين أعطت توافق كبير في قيم النتائج.

بِسْمِ اللَّهِ الرَّحْمَنِ الرَّحِيمِ

قُلْ لَوْ كَانَ الْبَحْرُ مِدَاداً لَّكَلِمَاتِ رَبِّي
لَنَفِدَ الْبَحْرُ قَبْلَ أَنْ تَنْفَدَ كَلِمَاتُ رَبِّي
وَلَوْ جِئْنَا بِمِثْلِهِ مَدَداً

صدق الله العظيم

سورة الكهف

آية (١٠٩)

CHAPTER ONE

Introduction

1-1 Introduction

The conventional energy sources, obtained from our environment, tend to exhaust with relative rapidity due to its irrational utilization by the humanity. This uncontrolled extraction of the natural energies, certainly will lead the harmony of our ecological system to the instability. It is important to point out, that if it occurs the recuperation of this system will be practically impossible.[1]

An a consequence of this possibility, the apprehension for a diminution of the petroleum sources, natural gas and natural resources of coal has been intensified. For this reason, the effort to find new sources of energy, to permit reduction in the utilization of the natural resources of fuel, became a challenge for all scientific and technological areas in the world, and especially for the electrical engineering area.[1]

Within this content, the solar energy appears as an important alternative to the increase of the energetic consumption of the planet, once that, the quantity of the energy from the sun that arrives on the earth surface in a day is ten times more than the total energy consumed for all the people of our planet during a year.[1]

Through the photovoltaic effect the energy contained in the sunlight can be converted directly into electrical energy. This method of energy conversion presents some advantages, such as:

- Simplicity.
- Does not exist any moving mechanical parts.
- Its modular characteristic offers large flexibility in the design and application of this kind of energy generator.
- Short time of installation and operation.
- High reliability and low maintenance.[1]

1-2 The Photovoltaic System

A photovoltaic (PV) system generates electricity by the direct conversion of the sun's energy into electricity. This simple principle involves sophisticated technology that is used to build efficient devices, namely solar cells, which are the key components of a PV system and requires semiconductor processing techniques in order to be manufactured at low cost and high efficiency. The understanding of how solar cells produce electricity from detailed device equations is beyond the scope of this research, but the proper understanding of the electrical output characteristics of solar cells is a basic foundation on which this research is built.[2]

A photovoltaic system is a modular system because it is built out of several pieces or elements, which have to be scaled up to build larger systems or scaled down to build smaller systems. Photovoltaic systems are found in the Megawatt range and in milliwatt range producing electricity for very different uses and applications: from a wristwatch to a communication satellite or grid connected.[2]

The elements and components of a PV system are the photovoltaic devices themselves, or solar cells packaged and connected in a suitable form and the

electronic equipment required to interface the system to the other system components, namely:

- storage element in standalone systems;
- the grid in grid-connected systems;
- AC or DC loads, by suitable DC/DC converters or DC/AC inverters.

Specific constraints must be taken into account for the design and sizing of these systems and specific models have to be developed to simulate the electrical behavior.[2]

1-3 Solar Cells

A solar cell is a PN junction device with no voltage directly applied across the junction. The solar cell converts photon power into electrical power and delivers this power to a load. Junction devices are usually known as photovoltaic cells or solar cells, although, the term is a misnomer in the sense that it is the current that is produced by the radiation photons and not the "voltage". The cell itself provides the source of EMF (by electric field produced by space charge). It is to be noted that photoelectric devices are electrical current sources driven by a flux of radiation.[3]

Photovoltaic generation of power is caused by radiation that separates positive and negative charge carriers in absorbing material. In the presence of an electric field, these charges can produce a current for use in an external circuit. Such fields exist permanently at junctions or in homogeneities in materials as "built-in" electric fields and provide the required EMF for useful power production.[3]

1-4 DC-DC Converters

DC-DC converters are widely used in power supply applications. Their ability to convert and stabilize dc voltage in a useful manner. DC-DC converters are often used together with rectifiers to convert ac voltage to a regulated dc. There are two basic converter topologies; the step-up (boost) and the step-down (buck). By combining them a number of different converters could be built. [4]

1-5 Multiple-Input DC-DC Converters

Recently, the zero-emission electric power generation system has been developed aggressively to exploit clean energy resources such as the solar array, wind generator, fuel cell, and so forth. In this case, the multiple-input dc-dc converter is useful to combine several input power sources whose voltage levels and/or power capacity are different and to get regulated output voltage for the load from them. [5]

1-6 Pspice

There are several circuit simulators available on the market such as SPICE, EMTP and SABER among several others [6]. In this thesis a spice simulator is used, pspice. A spice stands for simulation program with integrated circuit emphasis.

By modeling PV system components by their equivalent electronic circuits, one can use pspice to run simulation and verify the impact of different topologies and control techniques on the system. [7]

1-7 Literature Survey

Practical solar cells have only been available since the mid 1950's, but the phenomenon was discovered by French scientist Henri Becquerel in 1839.[4]

Charles Fritts (1883), an American inventor, described the first solar cells made from selenium wafers. In 1914 the existence of a barrier layer in PV devices was noted. Albert Einstein (1921) wins the Nobel Prize for his theories explaining the photovoltaic effect.[8]

Silicon solar cells are by far the most widely used and were first developed in 1954. Their main use has been for providing power for satellites since the 1957 launching of sputnik.[9]

In 1963 Sharp Corporation succeeds in producing silicon PV modules.[8]

Simulation programs running on digital computers allow computer designers to predict the operation of new chips, aerospace engineers to predict the characteristics of new air frames, and building designers to predict the thermal characteristics of new building, all without building anything.[10]

Dave Turcott et.al (2001), presents the current status of PV system software tools by surveying and categorizing some of the most common programs available today. Following this, it assesses the needs for future development in simulation and sizing software.[7]

Greg Waldo et.al (2002), their solar model consists of four "G table" voltage to current sources wired in parallel. The G table part contains the current vs. voltage values.[11]

Intusoft (2005), show that for simulator, the Si diode coupled with a photocurrent generator and ohmic resistance does the trick. It's assumed that solar cells are connected in series to achieve the desired open circuit voltage. Rather than connecting many diodes in series, it is convenient to scale the spice diode model.[12]

A.Aziz et.al (2006), focused in this paper on how to create a special library of some marketed solar panels in the orcad-pspice environment using the futures provided by the founder.[13]

Hirofumi Matsuo et.al (2004), show that in the zero-emission electric power generation system, a multiple-input DC-DC converter is useful to obtain the regulated output voltage from several input power sources such as a solar array, wind generator, fuel cell.[5]

Nicolas D. Benavides et.al (2005), discussed the use of a multiple-input buck-boost converter for budgeting power between different energy sources. It is shown mathematically that the idealized converter can accommodate arbitrary power commands for each input source while maintaining a prescribed output voltage. Power budgeting is demonstrated experimentally for a real converter under various circumstances, including a two-input (solar and line powered) system.[14]

1-8 Thesis Overviews

In chapter one of the thesis, issues related to PV system requirement are identified, also a historical review was presented to show the extent of research interest in this field.

Chapter two describes the principles and the electrical parameters of the PV cell (short circuit current, open circuit voltage, maximum power and fill factor), and then pspice model for PV cell was presented.

The simulation of the PV panel within the orcad-pspice simulator is presented in chapter three. The results from this chapter are used to investigate PV model validity as presented in chapter four.

Finally chapter five gives the conclusions and suggestions to continue and to extend this work in the future.

1-9 The aim of thesis

This thesis provides theoretical studies to build PV modeling techniques of type SP75 using equivalent electric circuits. The step down (buck) converter with two selective inputs is designed to test the PV model validity. After modeling and simulating the PV panel model, this model will be tested as input source to the buck converter and compare its results with that from battery.

CHAPTER TWO

Fundamental of Characteristics of the PV & Converters

2-1 Introduction

A majority of PV cells are Si semiconductor junction devices, thus in order to study the PV cells should have an understanding of the basics of the junction diodes. Details are also given of the PV cell parameters (Short Circuit Current I_{sc} , Open Circuit Voltage V_{oc} , Maximum power P_{max} and Fill Factor FF).

The I-V characteristics are analytically described and pspice models are introduced firstly for the simplest model. Then, it is generalized to take into account series resistance losses.

Also, the buck converter with multimode operation is presented here, in order to calculate the inductance and capacitance that is suitable for the optimum value of the PV model.

2-2 P-N Junction

The basic requirement for photovoltaic energy conversion is an electronic asymmetry in the semiconductor structure known as junction. When n-type and p-type semiconductors are brought in contact, then electrons from n-region near the junction would flow to the p-type semiconductor leaving behind a layer which is positively charged. Similarly holes will diffuse in the opposite direction leaving behind a negatively charged layer. A steady state is finally reached, resulting in a junction, which contains practically no movable

charges, hence the depletion region. Fig. 2-1 shows the energy levels in a p-n junction in state of photon absorption.

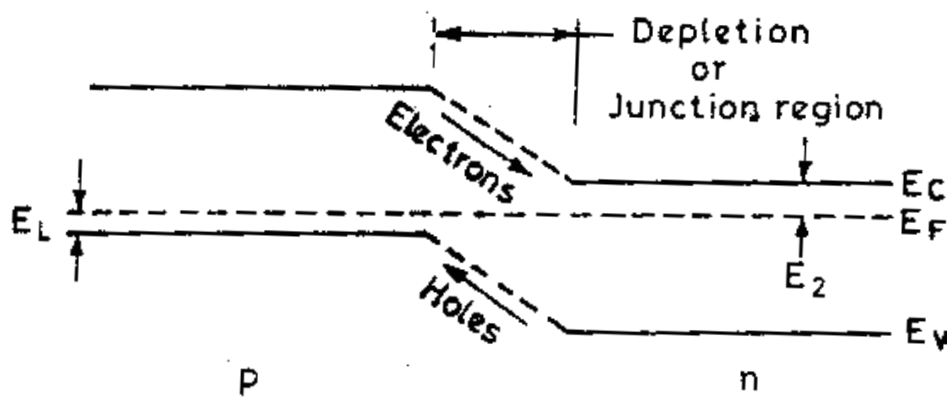


Figure 2-1: Energy levels in a p-n junction.

The p-n junction may be connected to a battery in two ways: i) In forward bias, the positive conventional circuit current passes from p to n material across a reduced band potential difference V_B as shown in fig. 2-2a. ii) In reverse bias in fig. 2-2b, the conventional positive current has an increased band potential difference V_B to overcome.

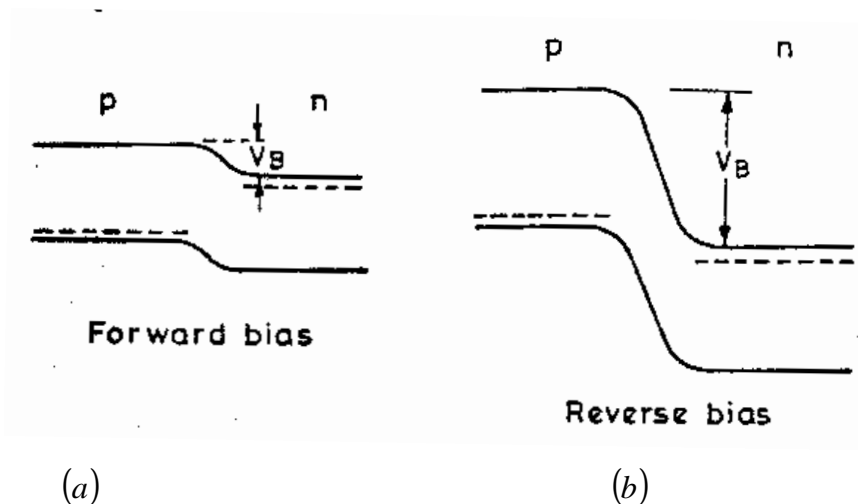


Figure 2-2: Energy level in a p-n junction with (a) Forward bias (b) Reverse bias.

Thermally or otherwise generated electrons and holes recombine after a typical relaxation time τ , having moved a typical diffusion length L through the lattice. In intrinsic material the relaxation time can be long, $\tau \sim 1$ s, but for commercial doped materials relaxation time are much shorter, $\tau \sim 10^{-2}$ to 10^{-8} s.

Electrons and holes may be generated thermally or by light, and become carriers in the material as shown in fig. 2-3. Minority carriers in the depletion region are pulled across electrostatically down their respective potential gradients. The minority carriers that cross the region become majority carriers in the adjacent layer. The passage of these carriers causes the generation current I_g which is mainly controlled by temperature in a given junction without illumination.

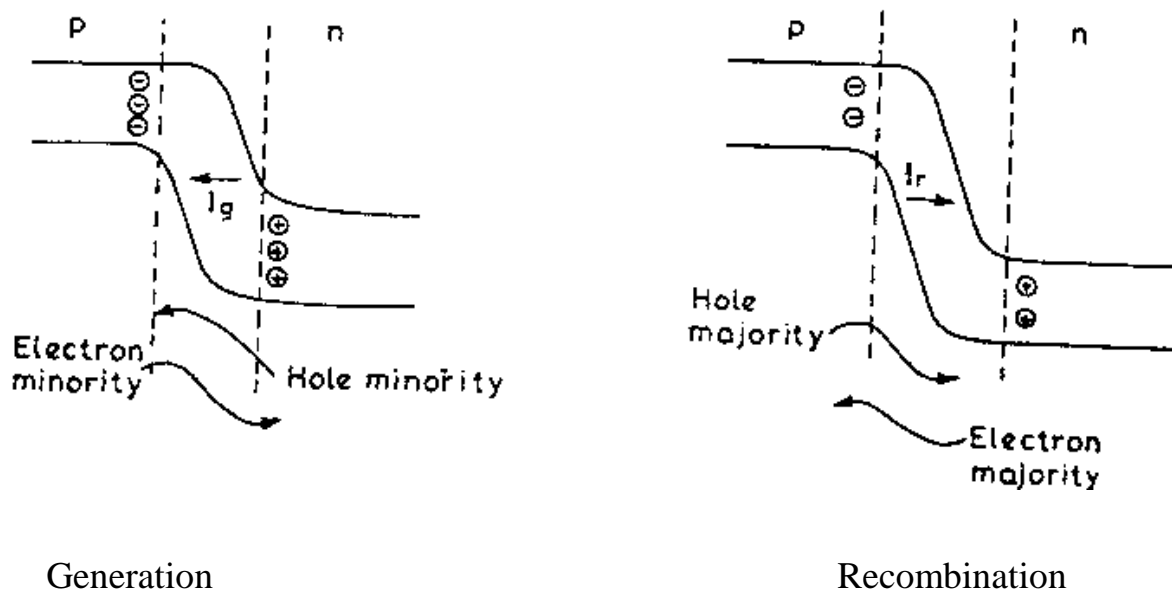


Figure 2-3: Generation and recombination current at p-n junction.

In an isolated junction, there cannot be overall imbalance of current across the depletion region. Thus, a reverse recombination current I_r of equal magnitude occurs from the bulk material, this restores the normal internal electric field. The band potential V_B is slightly reduced by I_r . The

recombination current I_r can be varied by external bias as explained in fig. 2-4.

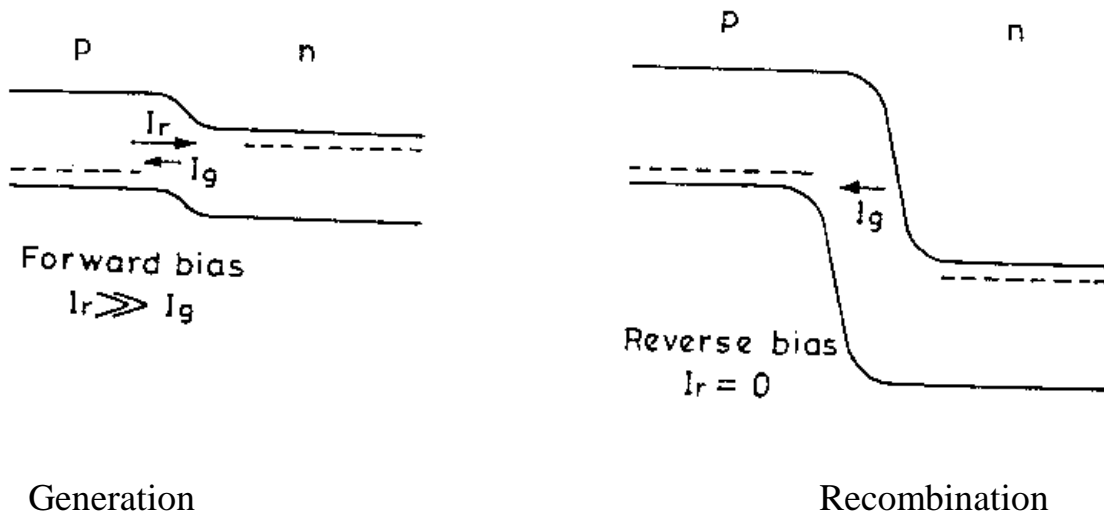


Figure 2-4: Generation and recombination currents with external bias.

2-2-1 P-N Junction Characteristics

The p-n junction characteristics have been given in fig. 2-5. With no external bias ($V = 0$).

$$I_r = I_g \quad (2-1)$$

With a forward bias of voltage V , the recombination current becomes an increased forward current.

$$I_r = I_g * \exp\left(\frac{eV}{KT}\right) \quad (2-2)$$

The total current (with no illumination) is,

$$ID = I_r - I_g = I_g * \left[\exp\left(\frac{eV}{KT}\right) - 1 \right] \quad (2-3)$$

The above equation is the Shockley equation and can be written as,

$$ID = I_0 \left[\exp\left(\frac{eV}{KT}\right) - 1 \right] \quad (2-4)$$

Where ($I_o = I_g = I_s$) is the saturation current under reverse bias, before breakdown occurs. It is also known as leakage or diffusion current, for good PV cells $I_o \sim 10^{-8} \text{ A.m}^{-2}$. Its value increases with temperature (as shown by dashed line in fig. 2-5). [3]

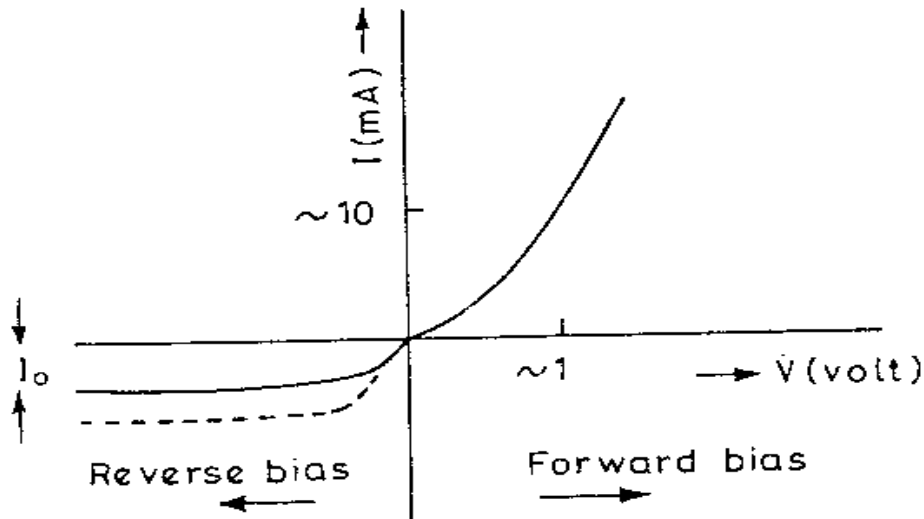


Figure 2-5: p-n junction dark characteristics.

2-3 The P-N Junction PV Cell

Consider the p-n junction with a resistive load shown in fig. 2-6 is illuminated, an interesting phenomenon can be observed. In the circuit there will be a flow of current caused by a voltage appearing at the terminals of the photovoltaic cell. This voltage is labeled V (photovoltage) and the results current I_L (photocurrent). The photovoltage arises from the generation of electron-hole pairs in the space-charge and the holes are swept into the p-side by the negative space charge. This movement charges the n-side negative and the p-side positively, with the resultant potential difference between the two sides being V . [15]

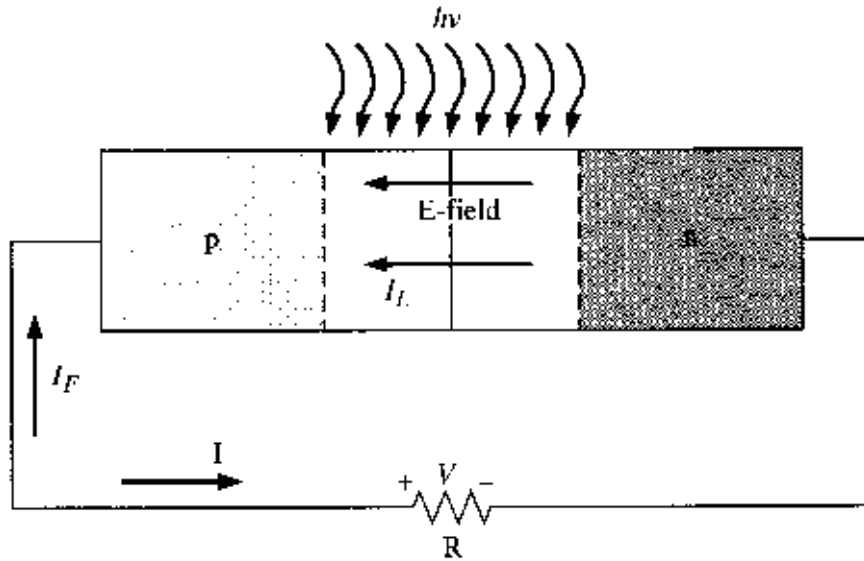


Figure 2-6: A p-n junction PV cell with resistive load.

Incident photon illumination can create electron-hole pairs in the space charge region that will be swept out producing the photocurrent I_L in the reverse bias direction as shown. This photocurrent produces a voltage drop across the resistive load which forward biases the p-n junction. The forward bias voltage produces a forward bias current I_F (acts the dark current as illustrated in section 2-2) as indicated in the figure. The net p-n junction current, in the reverse bias direction, is

$$I = I_L - I_F = I_L - I_S * \left[\exp\left(\frac{eV}{KT}\right) - 1 \right] \quad (2-5)$$

Where the ideal diode equation (or Shockley equation) has been used and the net p-n junction current acts the basic $I-V$ equation of PV cell. As the diode becomes forward biased, the magnitude of the electric field in the space charge region decreases, but does not go to zero or change direction. The photocurrent is always in the reverse bias direction and the net PV current is also always in the reverse bias direction. [16]

2-3-1 Photovoltaic Modeling

From the basic $I-V$ equation of the PV cell, pspice model for PV cell behaves like a silicon diode in parallel with a current source generator, explained by fig. 2-7; the magnitude of the current is proportional to the illumination.

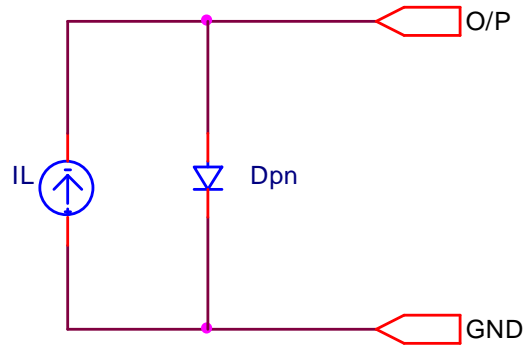


Figure 2-7: $I-V$ electric circuit representation of the PV cell.

2-3-2 The Fundamental Electric Parameters of the PV Cell

There are two limiting cases of interest seen from fig. 2-6. The short circuit condition occurs when $R = 0$ so that $V = 0$. The current in this case is referred to as the short circuit current, or [16]

$$I = I_{sc} = I_L \quad (2-6)$$

The second limiting case is the open circuit condition and occurs when $R \rightarrow \infty$. The net current is zero and the voltage produced is the open circuit voltage V_{oc} . The photocurrent is just balanced by the forward biased junction current so we have

$$I = 0 = I_L - I_s * \left[\exp\left(\frac{V_{oc}}{V_t}\right) - 1 \right] \quad (2-7)$$

where $V_t = \frac{KT}{e}$ thermal voltage

The open circuit voltage V_{oc} can be found as:

$$I_L = I_s * \left[\exp\left(\frac{V_{oc}}{V_t}\right) - 1 \right] \quad (2-8)$$

$$\frac{I_L}{I_s} = \exp\left(\frac{V_{oc}}{V_t}\right) - 1 \quad (2-9)$$

$$\frac{I_L}{I_s} + 1 = \exp\frac{V_{oc}}{V_t} \quad (2-10)$$

$$\text{Ln}\left(\frac{I_L}{I_s} + 1\right) = \frac{V_{oc}}{V_t} \quad (2-11)$$

$$V_{oc} = V_t * \text{Ln}\left(\frac{I_L}{I_s} + 1\right) \quad (2-12)$$

A plot of the diode current I as a function of the diode voltage V from eq. (2-5) is shown in fig. 2-8. Noted that the short circuit current and open circuit voltage point on the figure.

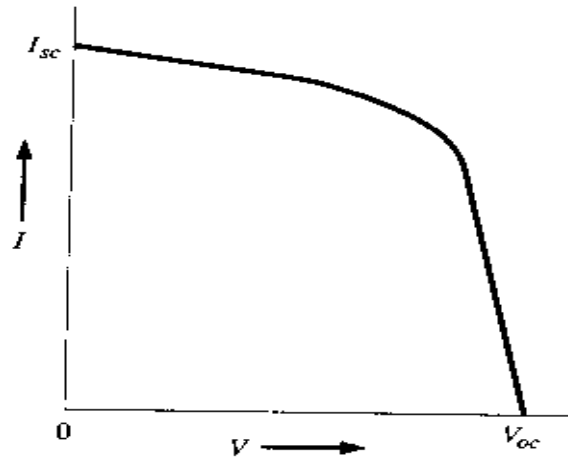


Figure 2-8: $I - V$ characteristics of a p-n junction PV cell.

The power delivered to the load is

$$P = I * V = I_L * V - I_s * \left[\exp\left(\frac{V}{V_t}\right) - 1 \right] * V \quad (2-13)$$

To find the current and voltage which will deliver the maximum power (M_{pp}) to the load by setting the derivative equal to zero, or $\frac{dP}{dV} = 0$.

$$\frac{dP}{dV} = 0 = I_L - I_s \left[\exp\left(\frac{V_m}{V_t}\right) - 1 \right] - I_s \frac{V_m}{V_t} \exp\left(\frac{V_m}{V_t}\right) \quad (2-14)$$

$$I_L + I_s - I_s \left(1 + \frac{V_m}{V_t} \right) \exp\left(\frac{V_m}{V_t}\right) = 0 \quad (2-15)$$

$$\frac{I_L + I_s}{I_s} = \left(1 + \frac{V_m}{V_t} \right) \exp\left(\frac{V_m}{V_t}\right) \quad (2-16)$$

$$\left(1 + \frac{V_m}{V_t} \right) \exp\left(\frac{V_m}{V_t}\right) = 1 + \frac{I_L}{I_s} \quad (2-17)$$

Fig. 2-9 shows the maximum power rectangle where V_m is the optimum voltage which produces the maximum power and I_m is the current when, $V = V_m$. [16]

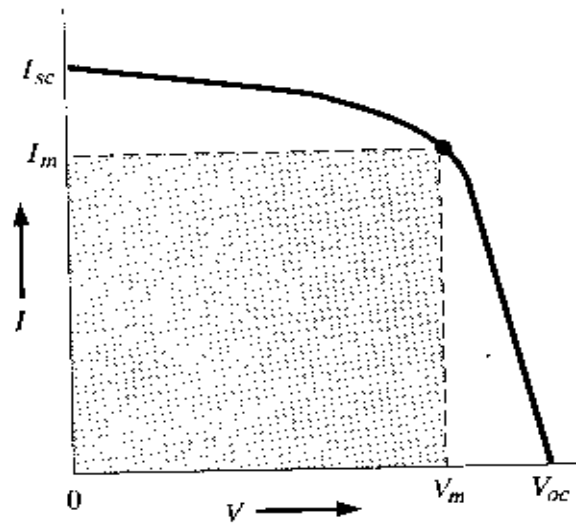


Figure 2-9: Maximum power rectangle of the PV cell $I - V$ characteristics.

The maximum power delivered is represented by the area of the largest rectangle that can be fitted under the curve. The squareness of the characteristic depends on the quality of the junction and the internal series resistance of the device. A measure of the squareness is the "fill factor", which is define [17]

$$FF = \frac{V_m * I_m}{I_{sc} * V_{oc}} \quad (2-18)$$

2-3-3 The dark & illuminated $I - V$ characteristics

Practically, the electric current generated in the semiconductor is extracted by metal contact to the front and rear of the cell. Then, the total series resistance of the cell can be expressed as [3]

$$R_s = R_{cp} + R_{bp} + R_{cn} + R_{bn} \quad (2-19)$$

Where R_{cp} is the metal contact to p-type semiconductor resistance; R_{bp} the bulk p-type resistance (bulk of p-type region is where most of electron/hole pairs are generated by the absorption of light and where minority carriers (electrons) are transported by diffusion and partially lost by recombination); R_{cn} the contact to n-type semiconductor resistance and R_{bn} the bulk n-type resistance.

In addition, a shunt path may exist for current flow across the junction named by I_p due to surface effect or poor junction region. This alternate path for current constitutes a shunt resistance R_p across the junction [3]. Then, the representation of the electric diagram for this state is shown in fig. 2-10.

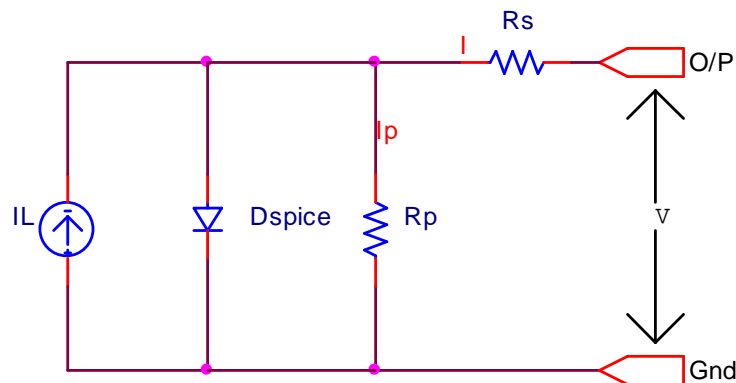


Figure 2-10: The generalized circuit diagram with shunt path R_p .

And the current equation of PV cell is given by Eq.(2-5)

$$I = I_L - I_s * \left[\exp\left(\frac{V_{pn}}{V_t}\right) - 1 \right] - I_p \quad (2-20)$$

where V_{pn} is the voltage appearing on the p-n junction device, as well as,

$$V_{pn} = I_p * R_p$$

Applying Kirchoff's voltage law to the output PV cell containing on R_s , R_p & V to find the value of V_{pn} & I_p

$$I_p * R_p - V - I * R_s = 0 \quad (2-21)$$

$$I_p = \frac{V + I * R_s}{R_p} \quad (2-22)$$

$$V_{pn} = V + I * R_s \quad (2-23)$$

Substitute the value of I_p & V_{pn} in eq.(2-20), the $I-V$ equation is become;[3]

$$I = I_L - I_s * \left[\exp\left(\frac{V + I * R_s}{V_t}\right) - 1 \right] - \frac{V + I * R_s}{R_p} \quad (2-24)$$

And $I-V$ characteristics of eq. (2-24) is shown in fig. 2-11.

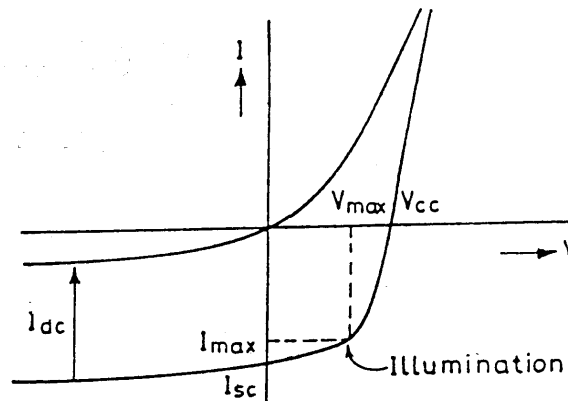


Figure 2-11: $I-V$ characteristics of a solar cell.

For good solar cell, the series resistance R_s should be very small and the shunt (parallel) resistance R_p should be very large. For commercial PV cells R_p are much greater than the forward resistance of a diode so that it can be

neglected and only R_s are of interest [3], then the final ($I-V$) equation of the output PV cell is given below ;

$$I = I_L - I_s * \left[\exp\left(\frac{V + I * R_s}{V_t}\right) - 1 \right] \quad (2-25)$$

The following are few of the characteristics parameters that have been discussed. [3]

The optimum load resistance $RL(P_{\max}) = R_{p \max}$ is connected, if the PV generator is able to deliver maximum power.

$$P_{\max} = V_{p \max} * I_{p \max} \quad (2-26)$$

And
$$R_{p \max} = \frac{V_{p \max}}{I_{p \max}} \quad (2-27)$$

The efficiency is defined as;

$$\eta = \frac{P}{\phi} \quad (2-28)$$

$P = V \times I$, is the power delivered by PV generator.

$\phi = I_t \times A$, is the solar radiation falling on the PV generator.

I_t is the solar intensity and A is the surface area irradiation. [3]

By neglect the shunt resistance R_p for above reason, the final generalized solar cell circuit diagram is shown in fig. 2-12.

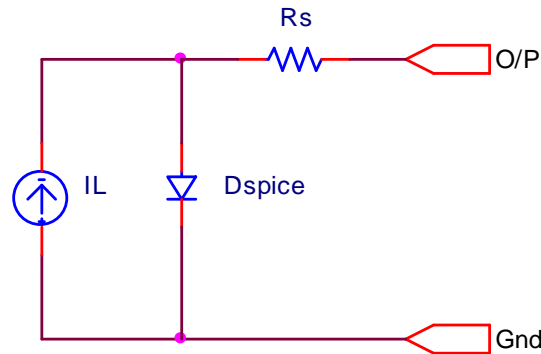


Figure 2-12: Final representation of the electric circuit of the PV cell.

2-4 PV Modules

Practically, after testing solar cells under test conditions and sorting to match current and voltage, about 36 solar cells are interconnected and encapsulated to form *a module*. Module consists of the following components:

- Front cover low iron tempered glass.
- Encapsulant, transparent, insulating, thermoplastic polymer, the most widely used one is EVA (ethylene vinyl acetate).
- The solar cell and metal interconnected.
- Back cover usually a foil of tedlar or Mylar.

Cells are usually mounted in modules and multiple modules are used in *arrays*. Individual modules may have cells connected in series and parallel combinations to obtain the desired voltage and currents. Arrays of modules may also be arranged in series and parallel. For identical modules or cells connected series, the voltages are added, while when connected in parallel the currents are added.[3]

The SP75 module is a solar panel made of mono crystalline silicon. It consists of 36 solar cells connected in series (Fig. 2-13). The surface of each solar cell is about $125\text{mm} \times 125\text{mm}$. Module SP75 can deliver 75 Watts under 17 volts (test standards condition TSC). The module surface is $120\text{cm} \times 52.7\text{cm}$.

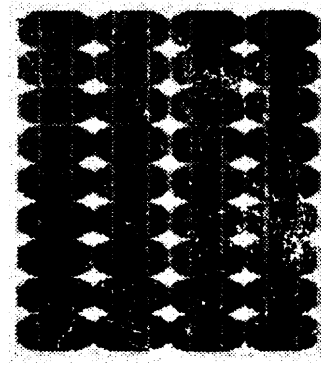


Figure 2-13: Solar panel SP75.

The electric characteristic of this panel under TSC is described in table 1. Thus, it appears that panel SP75 can deliver, in the TSC, 75W, 4.41A under an optimum voltage of 17V. [13] [AppendixB]

Maximal power	75W
Optimal voltage	17V
Optimal current	4.41A
Open circuit voltage	21.7V
Short circuit current	4.8A

Table 2-1: Electric characteristics of the panel SP75 under TSC.

2-5 Step-Down (Buck) Converter

Step-down converter as shown in fig. 2-14 converts a high input voltage to a lower output one. The ratio $\frac{ton}{T}$ determines the level of step down.

$$V_o = \frac{ton}{T} * V_d \quad (2-29)$$

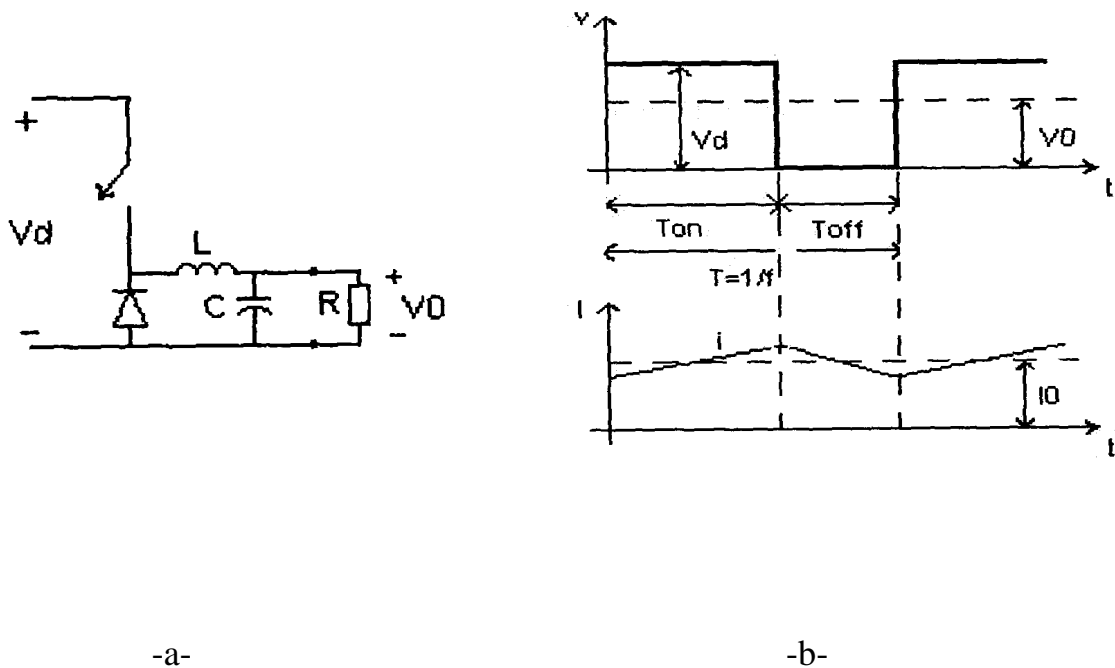


Figure 2-14: (a) Step down converter circuit. (b) Converter voltage and current waveforms.

It is worth noting that the output voltage is linearly depending of the time t_{on} . This makes it very easy to obtain a desired voltage. The low pass filter is used for different reasons. The switch produces high frequency ripple which the filter is low impedance. It is important to choose the cutoff frequency of the filter much lower than the switching frequency. Most applications don't accept that the voltage is zero at the time t_{off} . For this reason the low pass filter smoothes the voltage. The capacitance tries to stabilize the voltage and the inductance is trying to maintain a certain current. If the load isn't purely resistive (this is almost impossible to have) a free-wheel diode is needed. It is anyway needed when a low pass filter is used. The diode conducts the current that is charged in all inductances, at the time t_{off} . The inductance in the low pass filter is limiting the efficiency due to the resistance in the coils. The efficiency is usually quite good, ~90%. [4]

2-5-1 Continuous-Conduction Mode

Fig. 2-15 shows the waveforms for the continuous-conduction mode of operation where the inductor current flows continuously [$i_L(t) > 0$]. When the switch is on for time duration t_{on} , the switch conducts the inductor current and the diode becomes reverse biased. This results in a positive voltage $V_L = V_d - V_o$ across the inductor in fig. 2-15a. This voltage causes a linear increase in the inductor current i_L . [18]

When the switch is turned off, because of the inductive energy storage, i_L continue to flow. This current now flows through the diode, and $v_L = -V_o$ in fig. 2-15b.

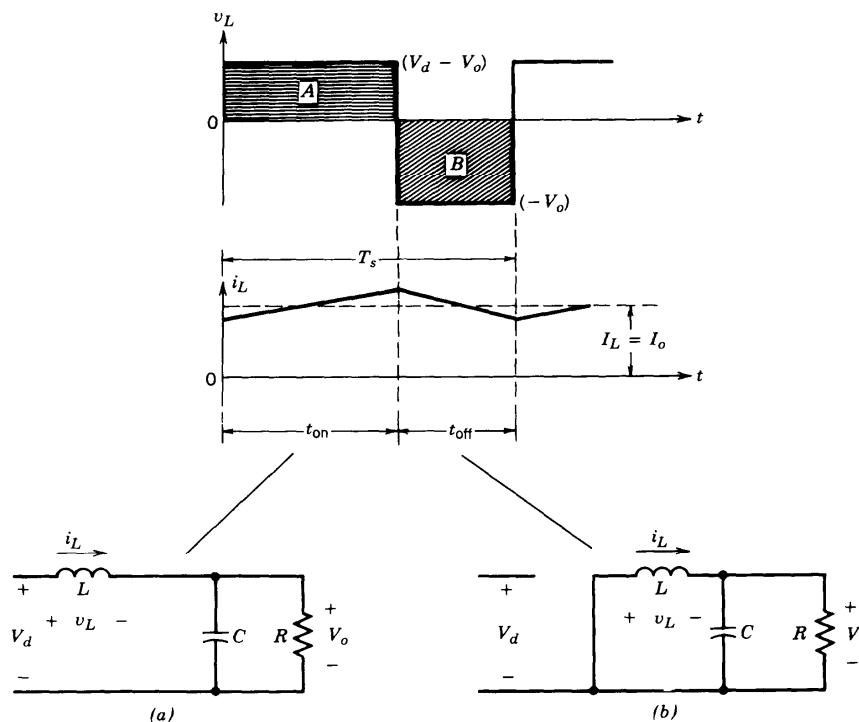


Figure 2-15: Step-down converter circuit states: (a) switch on (b) switch off.

Since in steady state operation the waveform must repeat from one time period to the next, the integral of the inductor voltage v_L over one time period must be zero, where $T_s = t_{on} + t_{off}$: [18]

$$\int_0^{T_s} v_L dt = \int_0^{t_{on}} v_L dt + \int_{t_{on}}^{T_s} v_L dt = 0 \quad (2-30)$$

In fig. 2-15, the foregoing equation implies that the area A and B must be equal therefore,

$$(V_d - V_o)t_{on} = V_o(T_s - t_{on}) \quad (2-31)$$

or

$$\frac{V_o}{V_d} = \frac{t_{on}}{T_s} = D \quad (2-32)$$

Therefore, in this mode, the voltage output varies linearly with the duty ratio of the switch for a given input voltage. It does not depend on any other circuit parameter.

Neglecting power losses associated with all the circuit elements, the input power P_d equals to the output power P_o : [18]

$$P_d = P_o \quad (2-33)$$

Therefore,

$$V_d * I_d = V_o * I_o \quad (2-34)$$

and

$$\frac{I_o}{I_d} = \frac{V_d}{V_o} = \frac{1}{D} \quad (2-35)$$

Therefore, in the continuous-conduction mode, the step-down converter is equivalent to a dc transformer where the turn's ratio of this equivalent transformer can be continuously controlled electronically in a range of 0-1 by controlling the duty ratio of the switch.

2-5-2 Boundary between Continuous and Discontinuous Conduction

At the edge of the continuous-current conduction mode, fig. 2-16a shows the waveform for v_L and i_L . Being at the boundary between the continuous and the discontinuous mode, by definition, the inductor current i_L goes to zero at the end of the off period.

At the boundary, the average inductor current, where the subscript B refers to the boundary, is [18]

$$I_{LB} = \frac{1}{2} i_{L, peak} = \frac{t_{on}}{2L} (V_d - V_o) = \frac{DT_s}{2L} (V_d - V_o) = I_{oB} \quad (2-36)$$

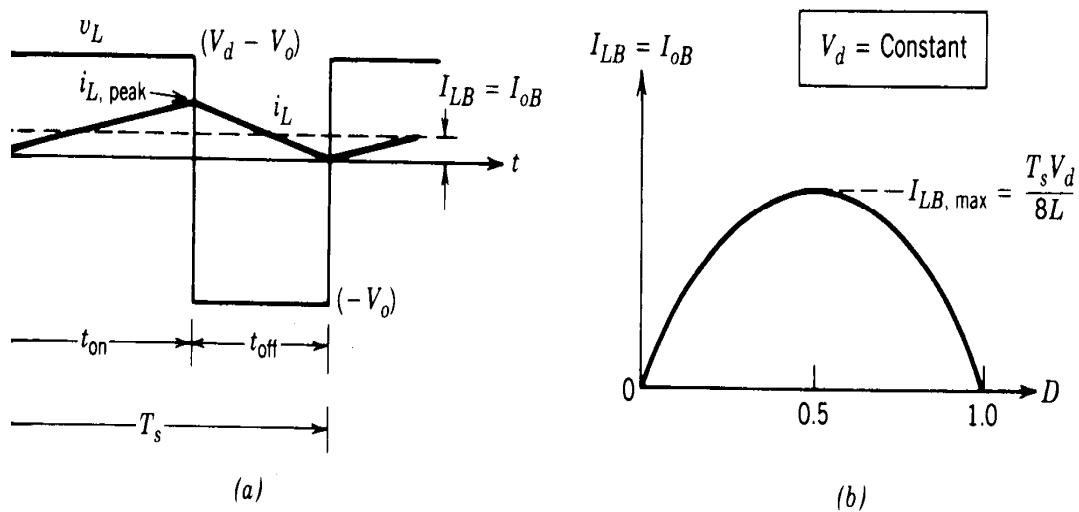


Figure 2-16: Current at the boundary of continuous-discontinuous Conduction:
 (a) current waveform: (b) I_{LB} versus D keeping V_d constant.

Therefore, during an operating condition (with a given set of values for T_s, V_d, V_o, L and D), if the average output current (and, hence, the average inductor current) becomes less than I_{LB} given by eq. (2-36), and then i_L will become discontinuous. [18]

2-5-3 Discontinuous-Conduction Mode

In some application, V_d remains essentially constant and V_o is controlled by adjusting the converter duty ratio D .

Since $V_o = D * V_d$, the average inductor current at the edge of the continuous-discontinuous mode from eq. (2-36) is [18]

$$I_{LB} = \frac{T_s V_d}{2L} D(1-D) \quad (2-37)$$

Using this equation, we find that fig. 2-16b shows the plot of I_{LB} as a function of the duty ratio D , keeping V_d and all other parameters constant. It shows that the output current required for a continuous-conduction mode is maximum at $D = 0.5$:

From eq. (2-37) taking the differential with respect to D : [18]

$$\frac{dI_{LB}}{dD} = \frac{T_s V_d}{2L} (1-2D) = 0 \quad (2-38)$$

Substitute the value of D from eq. (2-38) in eq. (2-37)

$$I_{LB,\max} = \frac{T_s V_d}{8L} \quad (2-39)$$

From eq. (2-37) and eq. (2-39)

$$I_{LB} = 4I_{LB,\max} D(1-D) \quad (2-40)$$

Next the voltage ratio V_o/V_d will be calculated in the discontinuous mode.

Let us assume that initially the converter is operating at the edge of continuous conduction as in fig. 2-16a, for a given values of T, L, V_d , and D . If these parameters are kept constant and the output load power is decreased (i.e., the load resistance goes up or lighter load), then the average inductor current will decrease. As shown in fig. 2-17, this dictates a higher value of V_o than before and results in a discontinuous inductor current.

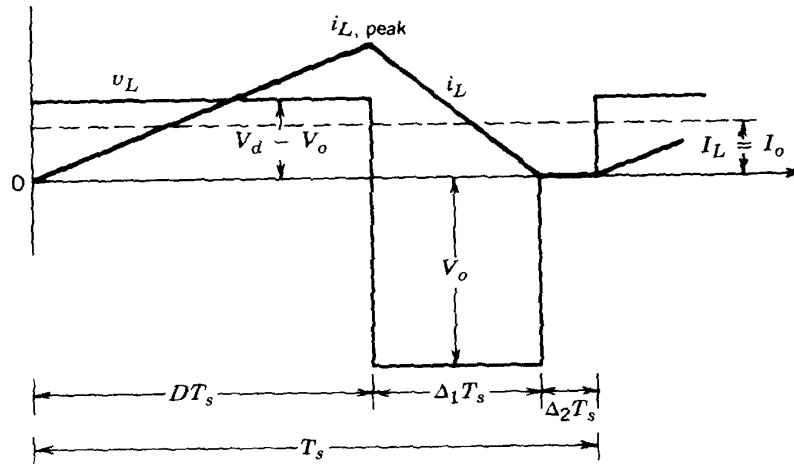


Figure 2-17: Discontinuous conduction in step-down converter.

During the interval $\Delta_2 T_s$ where the inductor current is zero, the power to the load resistance is supplied by the filter capacitor alone. The inductor voltage v_L during this interval is zero. Again, equating the integral of the inductor voltage over one time period to zero yields

$$(V_d - V_o)DT_s + (-V_o)\Delta_1 T_s = 0 \quad (2-41)$$

$$\therefore \frac{V_o}{V_d} = \frac{D}{D + \Delta_1} \quad (2-42)$$

where $D + \Delta_1 < 1$. From fig. 2-17,

$$i_{L, peak} = \frac{V_o}{L} \Delta_1 T_s \quad (2-43)$$

Therefore,

$$I_o = i_{L, peak} \frac{D + \Delta_1}{2} \quad (2-44)$$

using eq. (2-43)

$$I_o = \frac{V_o T_s}{2L} (D + \Delta_1) \Delta_1 \quad (2-45)$$

using eq. (2-42)

$$I_o = \frac{V_d T_s}{2L} D \Delta_1 \quad (2-46)$$

using eq. (2-39)

$$I_o = 4I_{LB, \max} D \Delta_1 \quad (2-47)$$

$$\therefore \Delta_1 = \frac{I_o}{4I_{LB, \max} D} \quad (2-48)$$

From eqs. (2-42) and (2-48)

$$\frac{V_o}{V_d} = \frac{D^2}{D^2 + \frac{1}{4} \left(\frac{I_o}{I_{LB, \max}} \right)} \quad (2-49)$$

Fig. 2-18 shows the step down converter characteristic in both modes of operation for a constant V_d . The voltage ratio (V_o/V_d) is plotted as a function of $I_o/I_{LB, \max}$ for various values of duty ratio using eqs. (2-32) and (2-49). The boundary between the continuous and the discontinuous mode, shown by the dashed curve, is established by eqs. (2-32) and (2-40). [18]

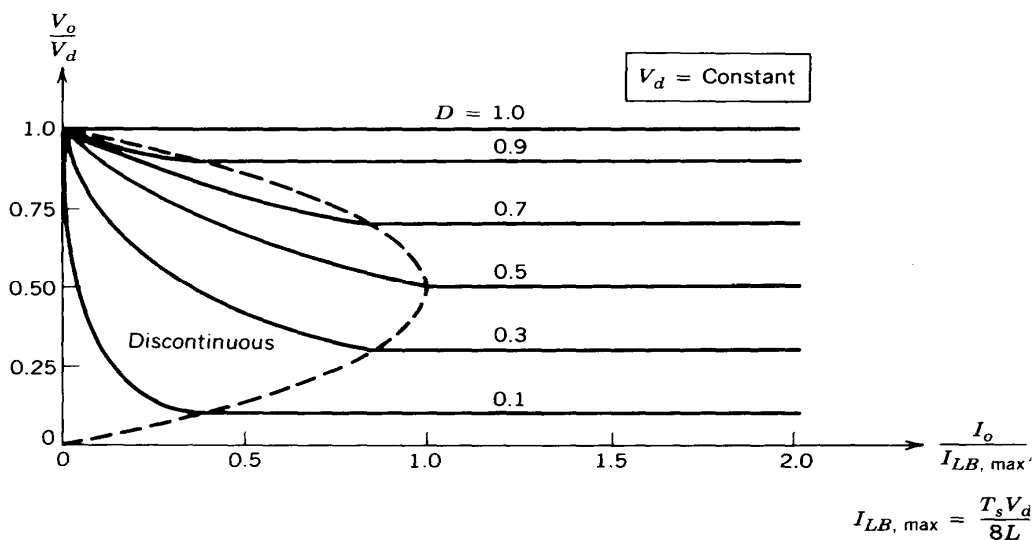


Figure 2-18: Step-down converter characteristics keeping V_d constant.

2-5-4 Output Voltage Ripple

The ripple in the output voltage with a practical value of capacitance can be calculated by considering the waveforms shown in fig. 2-19 for a continuous-conduction mode of operation. Assuming that all of the ripple component in i_L flows through the capacitor and its average component flow through the load resistor, the shaded area in fig. 2-19 represents an additional charge ΔQ . Therefore, the peak-to-peak voltage ripple ΔV_o can be written as [18]

$$\Delta V_o = \frac{\Delta Q}{C} = \frac{1}{C} \frac{1}{2} \frac{\Delta I_L}{2} \frac{T_s}{2} \quad (2-50)$$

From fig. 2-15 during t_{off}

$$\Delta I_L = \frac{V_o}{L} (1-D) T_s \quad (2-51)$$

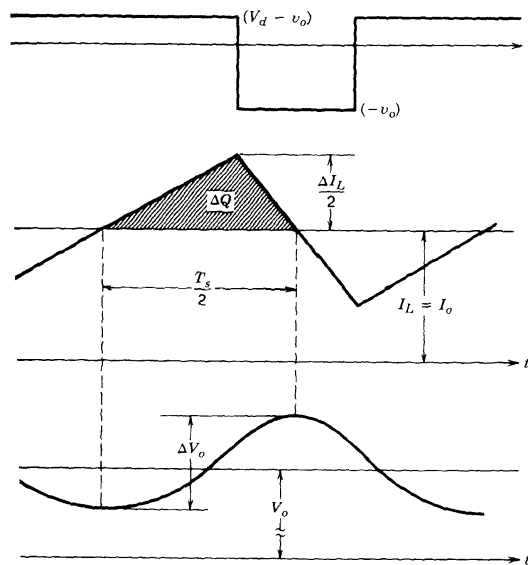


Figure 2-19: Output voltage ripple in a step-down converter.

Therefore, substituting ΔI_L from eq. (2-51) into the previous equation gives

$$\Delta V_o = \frac{T_s}{8C} \frac{V_o}{L} (1-D) T_s \quad (2-52)$$

$$\therefore \frac{\Delta V_o}{V_o} = \frac{1}{8} \frac{T_s^2 (1-D)}{LC} = \frac{\pi^2}{2} (1-D) \left(\frac{f_c}{f_s} \right)^2 \quad (2-53)$$

where switching frequency $f_s = 1/T_s$ and

$$f_c = \frac{1}{2\pi\sqrt{LC}} \quad (2-54)$$

Eq.(2-53) shows that the voltage ripple can be minimized by selecting a cutoff frequency f_c of the low-pass filter at the output such that $f_c \ll f_s$. Also, the ripple is independent of the output load power.

2-6 Output Control Circuit

All converters use some kind of switching for obtaining a desired output which is independent of the input. This means that the output of the switching is a pulse width modulated signal where the average voltage is the desired one as shown in fig. 2-20.

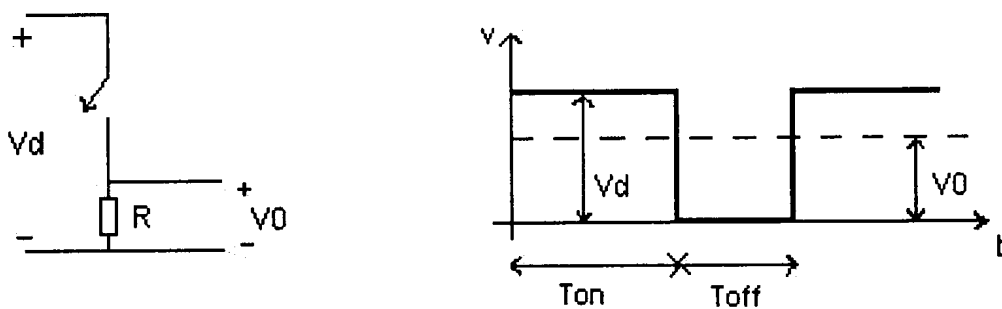


Figure 2-20: Simple step down converter.

In order to stabilize the output a control system is used. A reference voltage is compared with the actual output as shown in fig. 2-21. If there is a mismatch, the control system adjusts the duty cycle in the switching. This is made by an OP amplifier and a comparator. The OP detects the error in output voltage and compares it with a sawtooth voltage.

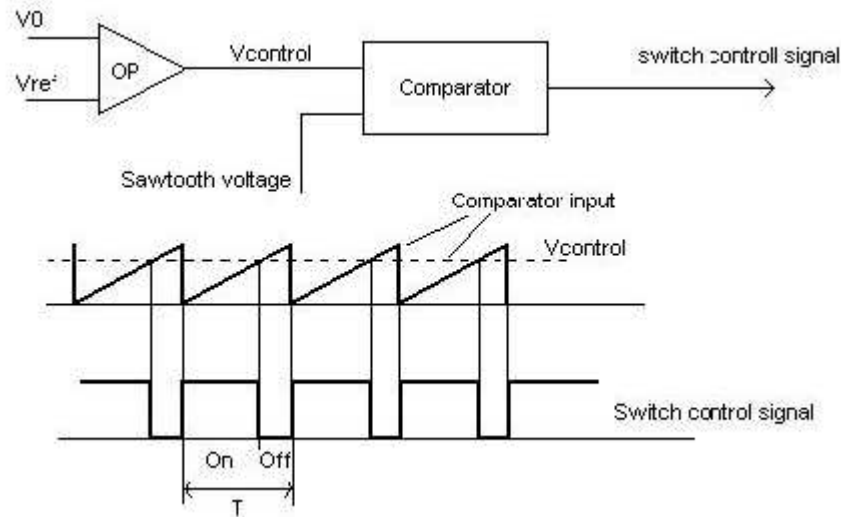


Figure 2-21: PWM circuit used for stabilizing the output voltage.

The switching frequency is often chosen in the range from a few kilohertz to some hundred kilohertz. This makes it possible to stay out of frequencies which could disturb other systems. With a good design and some low pass filtering the problem can be solved. [4]

2-7 A multiple Input DC-DC Converter

Most electrical systems are supplied by one kind of energy source. Whether it is batteries, wind, solar, etc. Certain special cases are powered by two sources, such as, uninterruptible power supplies.

The different sources such as PV cells and batteries will have different voltage and current characteristics. With multiple inputs, the energy source is diversified to increase reliability and utilization of renewable sources. An ideal multiple-input power supply could accommodate a variety of sources and combine their advantages automatically, such that the inputs are interchangeable. Such a converter could be relocated and still take advantage of the local environment, e.g., in some areas solar power would be readily accommodate, in others, utility power may be a specially reliable or inexpensive.[5]

CHAPTER THREE

PV Panel Simulation Results

3-1 Introduction

In this chapter the PV Panel has been simulated within the orcad-pspice simulator. Details are also given to the methods of measuring the panel parameters I_{sc} , R_s and I_s . Several techniques are described to create new components (PV), in the orcad-pspice simulator library which will be called directly by their equivalent circuits.

3-2 Panel Parameters Calculation

The entire cell is represented according to the model of fig. 2-10. The current generator (I_L) provides a short circuit current which is a function of the solar irradiation (P_{var}) according to an equation determined by the characteristics $I-V$ provided by the manufacturer:

$$I_{sc} = a \bullet P_{var} - b \quad (3-1)$$

where, a and b are constants which depend on PV cells.

Eq. (3-1) is similar to Eq. (2-25) with some modifications, V equal zero under short circuit current condition and become:

$$I_{sc} = I_L - I_s * \left[\exp\left(\frac{I_{sc} * R_s}{V_t}\right) - 1 \right] \quad (3-2)$$

where

$$I_L = a \bullet P_{var} \quad (3-3)$$

$$b = I_s * \left[\exp\left(\frac{I_{sc} * R_s}{V_t}\right) - 1 \right] \quad (3-4)$$

From the practical results obtained by A.Aziz et.al[13], the current crossing a cell could be described according to illumination $P_{var}(W/m^2)$:

$$I_{sc}(A) = 0.00481 \cdot P_{var} - 0.0125 \quad (3-5)$$

It should be noted that the test standard conditions (TSC) are defined by irradiance power (P_{var}) of $1000W/m^2$, a temperature of $25C^0$.

Therefore, $I_L = 4.81A$ (3-6)

3-3 Simulation of the PV panel

It is possible to simulate a column of PV cell and a panel in the orcad-pspice if the parameters I_L, I_s, R_s for a single cell are calculated.

The value of I_L (for single cell) is determined from eq. (3-6) in order to determine I_s and the circuit shown in fig. 3-1 is used, *Dspice* is a diode whose parameter I_s (saturation current) is calculated from simulation under open circuit voltage condition $V = V_{oc}$.

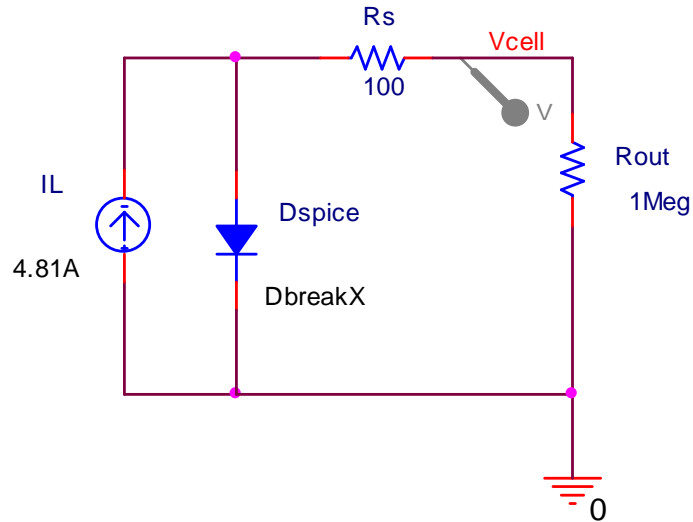


Figure 3-1: The circuit diagram used to determine I_s .

In order to eliminate the voltage drop across R_s , the PV cell terminal is connected to high resistance (R_{out}).

From Dc simulation result shown in fig. 3-2 ($I_s = 436.96\mu\text{A}$) at $V_{oc} = 0.602\text{V}$ (open circuit voltage for single cell).

According to the electrical characteristics of the panel SP75 (table 2-1) under test standard conditions the optimum load equal to $0.1069\text{m}\Omega$.

D_{breakX} (the pspice model of the diode) is built according to the results from fig. 3-2 ($I_s = 436.96\mu\text{A}$, $N = 1$, $R_s = 0.001\Omega$, $X_{TI} = 3$, $I_{KF} = 0\text{A}$, $E_G = 1.11\text{eV}$, $C_{jo} = 1\text{pF}$, $M = 0.3333$, $V_J = 0.75\text{V}$, $F_c = 0.5$, $I_{SR} = 0.1\text{pA}$, $N_R = 2$, $B_V = 100\text{V}$, $I_{BV} = 0.0001\text{A}$).

The last parameter R_s is represented as R_{val} in fig. 3-3 and simulated under optimum load resistance R_p (max). From Dc analysis results shown in fig. 3-4 $R_s = 13.95\text{m}\Omega$.

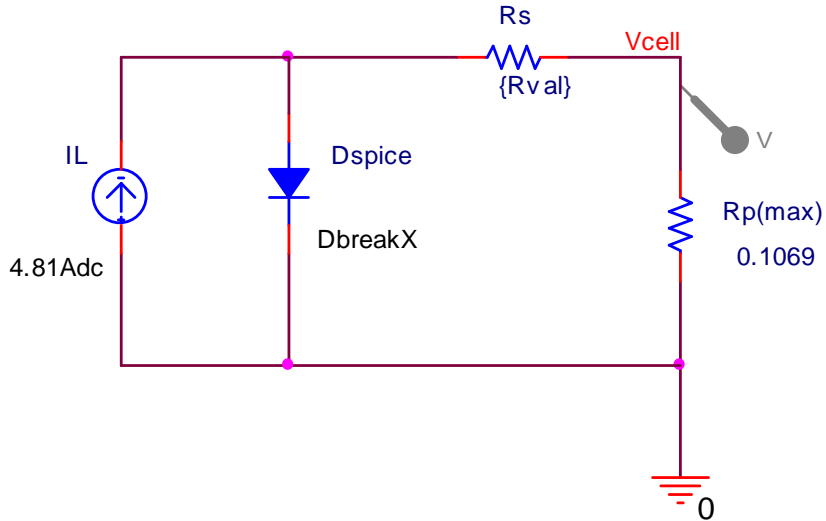


Figure 3-3: The circuit diagram used to determine R_s .

Now it is possible to define the PV panel (SP75) by associating 36 elementary cells in series as shown in fig. 3-5. Observe that the value of internal resistance R_s for whole model is the sum of the internal resistance of the entire cell; also is could be calculated in the same manner as in fig. 3-4. In both methods R_s equal to $500.946\text{m}\Omega$ as shown in fig. 3-6.

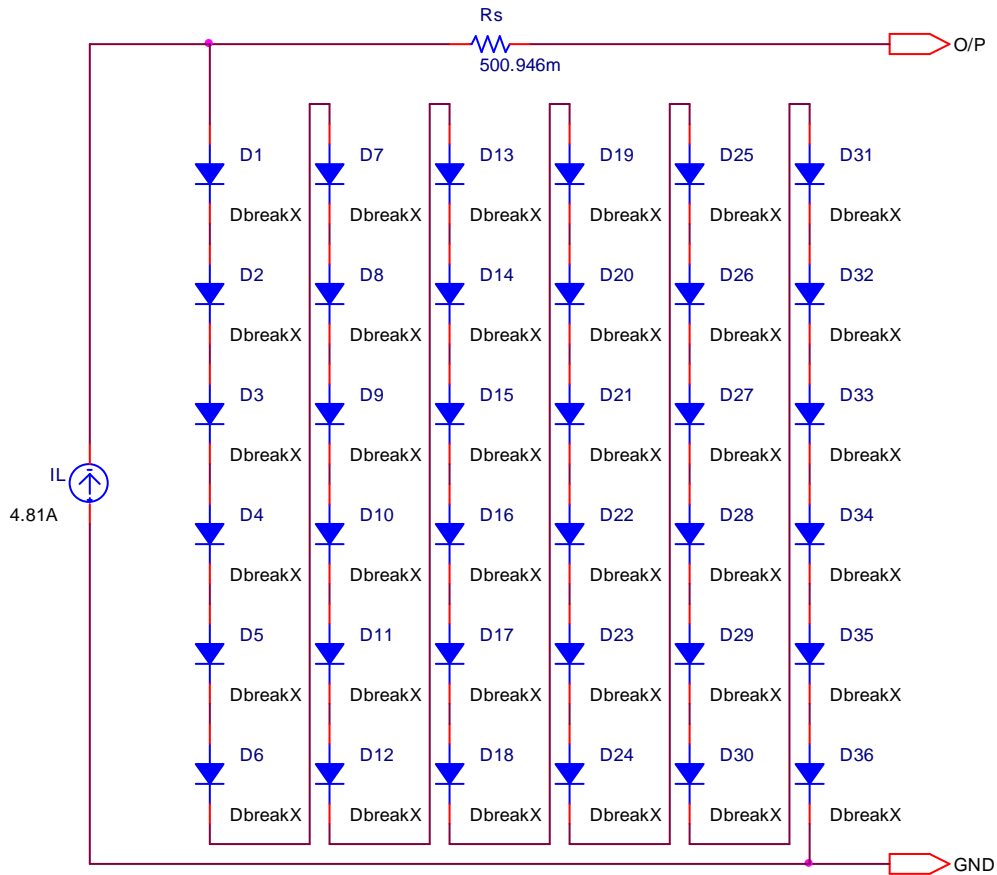


Figure 3-5: The electrical circuit of the model SP75.

3-4 Simulation Results

The model described in the previous paragraph has been implemented in the orcad-pspice. This model has been verified and used to find the optimal operation. Fig. 3-7 shows the current-voltage curve, obtained from the simulation (Dc analysis) of the PV model. The optimal load replaced by R_{break} to obtain all value of I and V.

The simulated model shows 21.7V open circuit voltage and 4.8A short circuit current at $25C^{\circ}$ with $1000W/m^2$ solar irradiation.

Next, the following figures (3-8) (3-9) depict the results of the simulation at different temperature and irradiation respectively.

The power vs. voltage plot is described on fig. 3-10. It reveals that the amount of power produced by the PV model varies greatly depending on its operating condition. It is important to operate the system at the maximum power point of PV model in order to exploit the maximum power from the model ($P = 75.953\text{W}$ at $V = 17\text{V}$).

The location of the maximum power point in the ($P-V$) plane is not known beforehand and always changes dynamically dependence on irradiance and temperature. Fig 3-11 shows the ($P-V$) curve at the irradiance value but with a higher temperature and fig. 3-12 shows the ($P-V$) curve under decreasing irradiance at the constant temperature (25C°). There are observable shift where the maximum power point occurred.

All the results are similar to the real characteristics; therefore its can be concluded that the simple pspice model of PV used here is valid.

3-5 Hierarchical Block

The model which explained previously is very large so to minimize it an integrated part (hierarchical block) has been considered as shown in fig. 3-13.

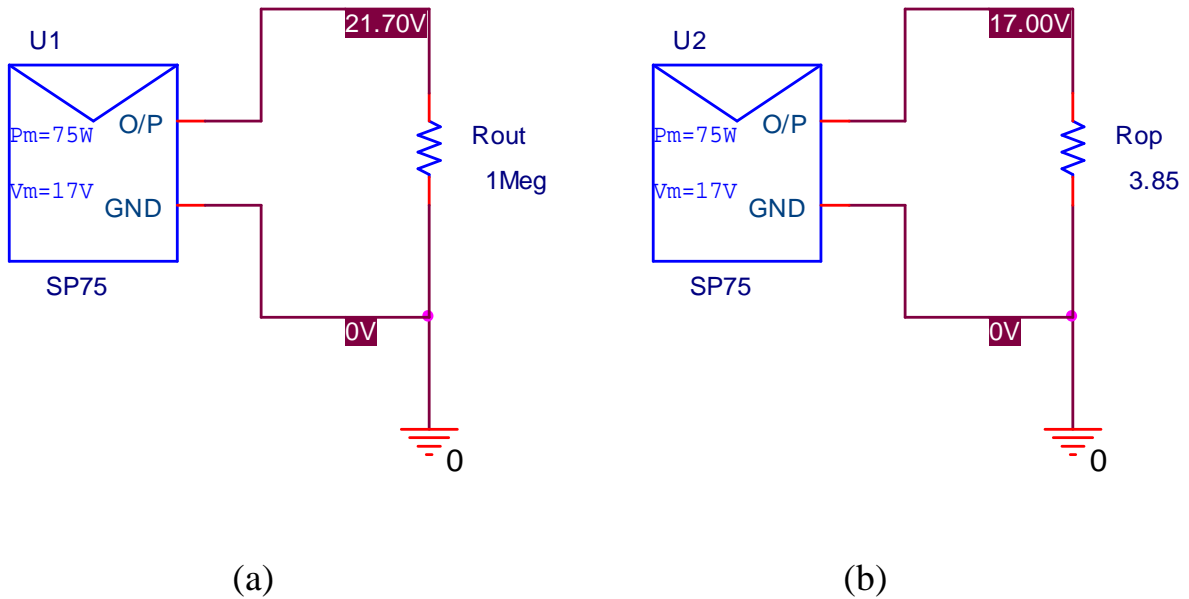


Figure 3-13: The hierarchical block (part) of SP75 in state of (a) open circuit voltage condition. (b) optimum load condition.

The results obtained from this integrated part (fig. 3-14, 3-15, 3-16, 3-17) and previous section are compatible. Therefore, the hierarchical block is used to define the PV panel model as integrated part into special library. This part will be called from that library to simulate the $(I-V)$ and $(P-V)$ characteristics of the PV model, as well as this part is used as a source of energy to the power circuits.

CHAPTER FOUR

Testing the PV Panel Model in Converter Circuit

4-1 Introduction

After modeling and simulating the PV panel model in the previous chapter. Here this model will be tested as input source to the buck converter and compare its results with that from battery.

4-2 Converter Circuit Design

The step down (buck) converter is designed for variable output voltage of (1.5V-12V), switching frequency (20 kHz), duty cycle (0.1- 0.7) and output power (1W- 41.6W). Fig. 4-1 shows the buck converter as represented in pspice.

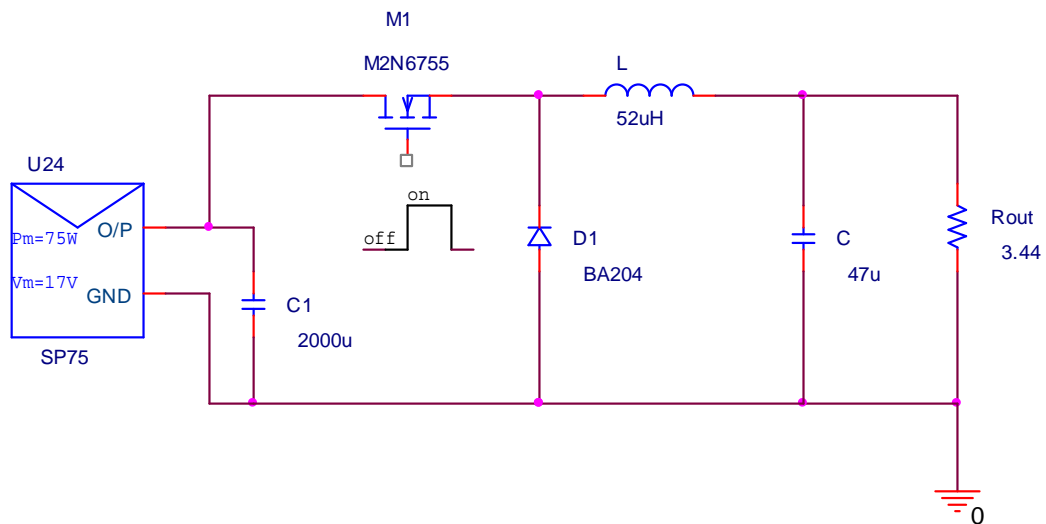


Figure 4-1: The step down converter configured in pspice.

This converter is tested by assuming V_d constant. Therefore, L and C are calculated according to eqs. (2-39) and (2-53) respectively.

The parameters of these two equations are calculated according to the panel model ($I-V$) curve shown in fig. 3-7. From that figure $V_{pv} = 19.8V$ at $2.4A$ ($I_{LB, \max}$). Therefore,

$$I_{LB, \max} \approx 2.4A$$

$$V_d = V_{pv} \approx 19.8V$$

$$T_s = 50\mu s$$

$$\therefore L \approx 52\mu H$$

The percentage ripple in the output voltage is usually specified to be less than 8%.

$$\Delta V_o = 0.08V_o$$

$$D = 0.6 \text{ at continuous mode condition}$$

$$T_s = 50\mu s$$

$$L = 52\mu H$$

$$C \geq 30\mu F$$

The important notice that the buck converter can match the load to the PV panel if the load is less than the optimum load for the PV panel [19].

The output diode D1 (BA204) conducts when the power switch turns OFF and provides a path for the inductor current. An important criteria for selecting the rectifier includes fast switching, breakdown voltage, current rating and low forward voltage drop to minimize power dissipation. The best solution for low voltage drop is usually a Schottky rectifier. [20]

Also, it should be noted that the input current (PV current) for the buck converter is of discontinuous (switching) nature. This results in an unstable operating point on PV panel which switches between M_{pp} and the open circuit and results in the loss of energy. Under such condition true maximum power point operation could never be achieved. To avoid this problem a large capacitor C1 is used at the input of the buck converter unit. This offers a stable operating point on the PV panel. The capacitor still introduces a switching frequency ripple on the PV panel voltage because of charging and discharging in every cycle. This ripple can be kept to a minimum acceptable value by using a large capacitor at the input. A $2000\mu F$ capacitor gives the satisfactory results. [19]

4-2-1 PWM Generator

This unit generates the signal with necessary duty ratio to drive the switching devices of the converter. The PWM generator is shown in fig. 4-2.

The error amplifier U10 (LM324) detects the error output results from the difference between the reference voltage (V_{ref}) and the actual voltage (V_{fb}); this error level is applied to the control terminal (pin5) of the 555 timer.

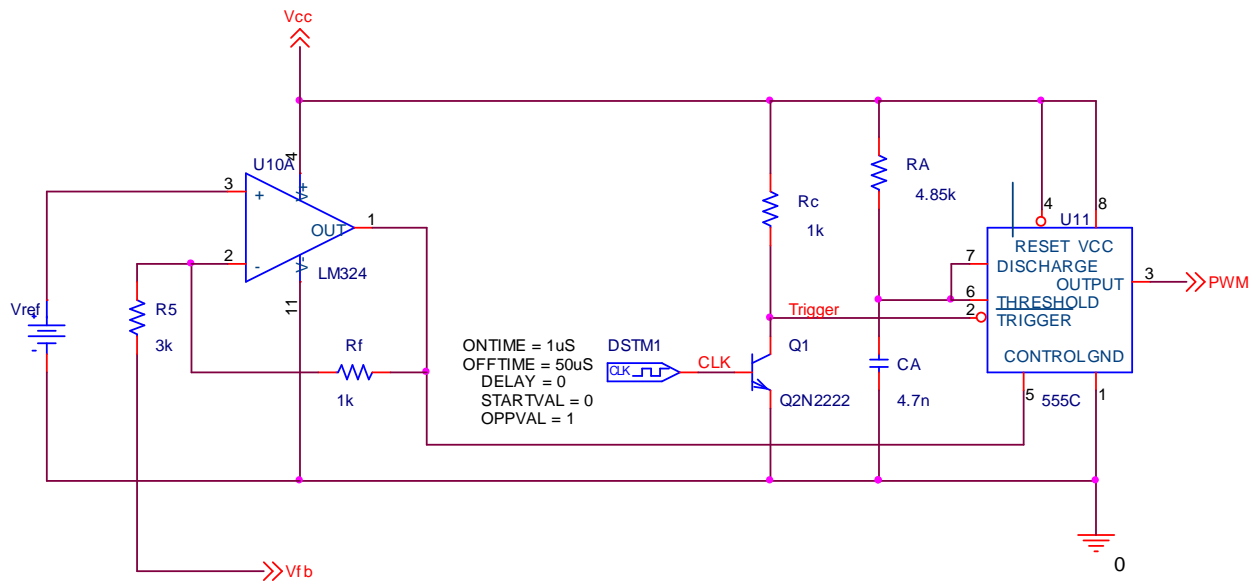


Figure 4-2: The complete system of the PWM generator.

The 555 timer is operated in monostable mode. Triggering the 555 timer in monostable mode with a continuous sequence of pulses allows the output pulse width to be modulated by changing the amplitude of a signal applied to the control input pin5. The trigger signal on pin2 causes the 555 timer output signal to go high. Retriggering will occur if the trigger pulse is hold low longer than the 555 timer output pulse width. The transistor Q1 (2N2222) is connected as explained in fig. 4-10, to configure the DC path to ground in state of the transistor Q1 is on and prevent the 555 timer from retriggering when the transistor is off (pin 2 equal to Vcc).

The resistor R_A and the capacitor C_A limited the output pulse width for 555 timer. These two elements are calculated according to the equation below;

$$T_{on} = 1.098R_A C_A$$

at $T_{on} = 25\mu s$, let $C_A = 4.7nF$ then $R_A = 4.85k\Omega$.

4-2-2 MOSFET Gate Drive Circuit

The output of the PWM signal is applied to the OP amplifier U19 (LM311) as shown in fig. 4-3. This OP amplifier supplied pulse of sufficient voltages and drove current to the gate of the switching device M1 (M2N6755) through a resistance R_g . The OP amplifier U19 represents the buffer circuit between the PWM generator and the gate of the MOSFET switch, the output of the gate drive act as open collector terminology. For this reason the resistor R_{c1} is connected between V_{cc} and the output terminal of U19 to get the train of pulses.

In the same manner OP amplifier U23 (LM311) is used to drive the second MOSFET M2 (M2N6755).

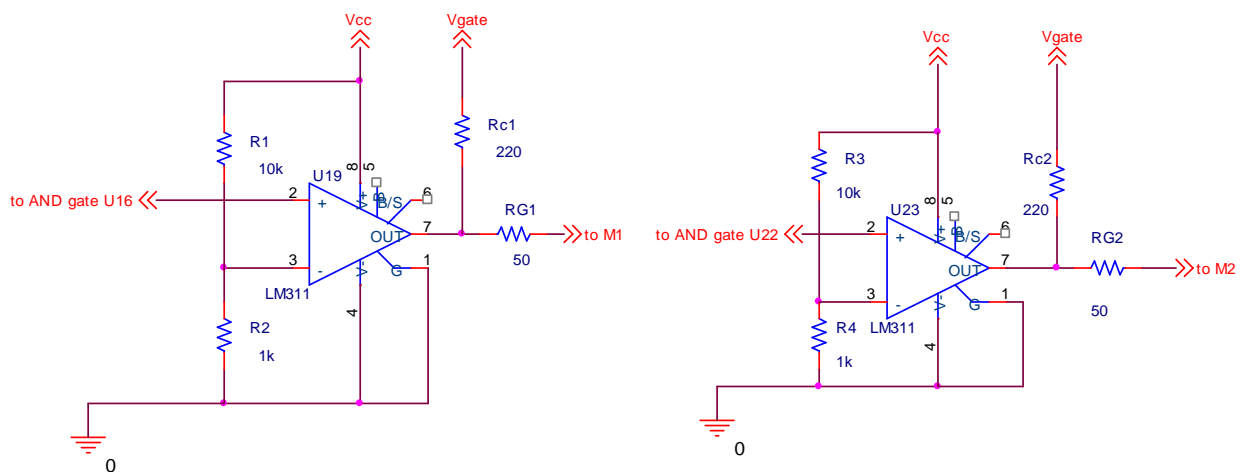


Figure 4-3: The gate drive circuit.

4-2-3 Sources Control Circuit

The circuit shown in fig. 4-4 represent the Demultiplexer logic circuit and there elements are U18A (CD4081B), U20A (4009A) and U21A (4001B).

This circuit performs the interchange between two sources (PV panel and battery). When V_4 equal zero the PV panel is active otherwise the other.

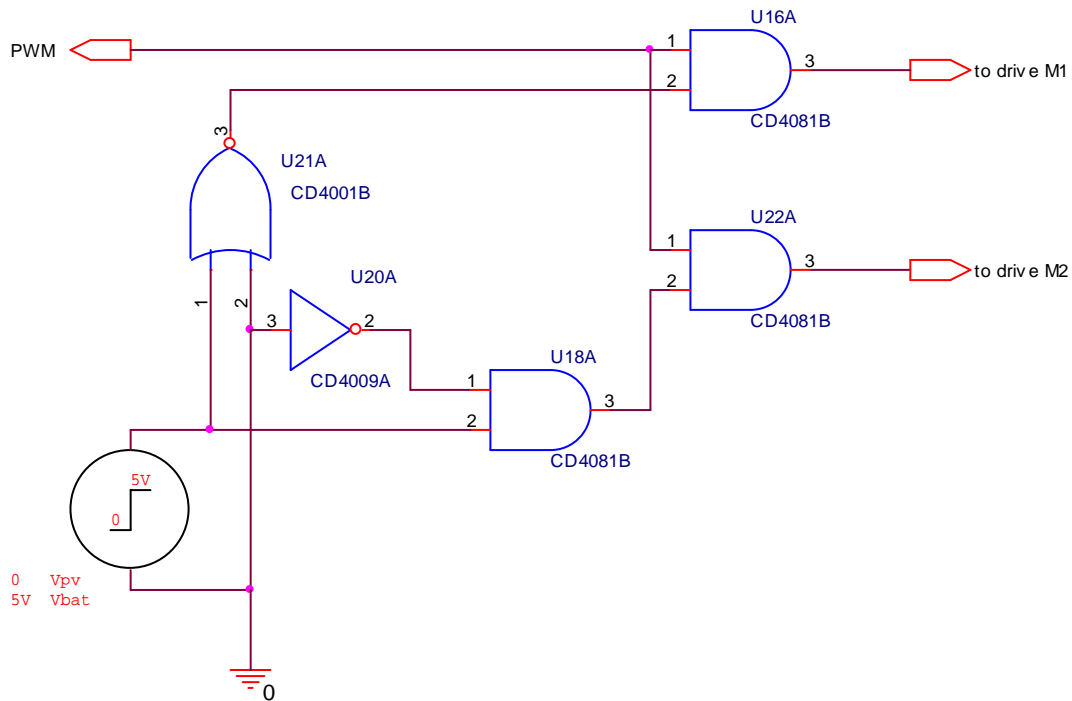


Figure 4-4: The sources control circuit.

4-3 The System Configuration

Fig. 4-5 shows the complete design of the two input PWM buck converter with interchange between the source operations, the parts of this system deal with enough description. In addition, the diodes D3 and D4 prevent the MOSFET switch M1 and M2 to conduct in depletion mode, respectively.

4-4 Two input buck converter simulation results

In this section, the waveforms obtained from transient simulation of buck converter for different modes of operation, boundary continuous and

discontinuous, are presented. Transient simulation of the converter system was carried out in orcad-pspice simulator.

The simulation waveform for a buck converter operates in the boundary modes are displayed in fig.4-6 through 4-11. Figure 4-6 gives the output voltage and current of the converter from the PV pspice model. Also fig. 4-7 gives the output voltage and current of the converter but from the battery. It is observed that the output voltage is equal to 8.5V and the output current equal to 2.4A in the two cases. The inductor voltage and current waveforms can be seen in the figures 4-8, 4-9 for PV pspice model and a battery respectively. The trigger signal of the 555 and its output (PWM signal) are shown in fig 4-10 for PV and 4-11 for battery.

In a similar manner the simulation results for a buck converter operates in continuous and discontinuous modes are satisfied in figure 4-12 through 4-23.

For all three modes figures, the simulation results for PV pspice model match closely the results obtained from the battery.

CHAPTER FIVE

Conclusions and Future Work

5-1 Conclusions

From the present study, can conclude the following:

1. This research described briefly how a PV panel consists of 36 cell connected in series was created in the orcad-pspice simulator library. Therefore, for a given panel, electric characteristics (voltage-current) can simulate by calling directly the panel of the orcad-pspice library. All the panel parameters were calculated before the model defined in orcad-pspice (like R_s , I_s). Also pspice model of diode, represent the elementary cell, was built by simulation (saturation current, identity factor, N_r , M ...).
2. The results shows that the PV model using the equivalent circuit in moderate complexity provides good matching with the real PV module.
3. At the same time a two input Dc-Dc converter, was built in pspice to prove the validity of the PV panel model. This is achieved by comparing the results of the converter with a dc battery to that with the PV panel model. The converter with two sources gave us a compatible result with a good agreement between them.

5-2 Future work

For future work, can recommend the introduction of the following open problems:

1. It is possible to symbolize a PV panel by associating 36 elementary cells in series and parallel.
2. Study the effect of shading or mismatch for one cell or more in PV panel.
3. Interfacing sources is important to consider, due to the different voltage and current characteristics of the PV panel and the battery.

List of figures

Figure 2-1	Energy levels in a p-n junction	9
Figure 2-2	Energy level in a p-n junction with (a) Forward bias (b) Reverse bias	9
Figure 2-3	Generation and recombination current at p-n junction	10
Figure 2-4	Generation and recombination currents with external bias	11
Figure 2-5	p-n junction dark characteristics	12
Figure 2-6	A p-n junction PV cell with resistive load	13
Figure 2-7	$I - V$ electric circuit representation of the PV cell	14
Figure 2-8	$I - V$ characteristics of a p-n junction PV cell	15
Figure 2-9	Maximum power rectangle of the PV cell $I - V$ characteristics	16
Figure 2-10	The generalized circuit diagram with shunt path R_p	17
Figure 2-11	$I - V$ characteristics of a solar cell	18
Figure 2-12	Final representation of the electric circuit of the PV cell	19
Figure 2-13	Solar panel SP75	21
Figure 2-14	(a) Step down converter circuit. (b) Converter voltage and current waveforms	22
Figure 2-15	Step-down converter circuit states: (a) switch on (b) switch off	23
Figure 2-16	Current at the boundary of continuous-discontinuous Conduction:(a) current waveform: (b) I_{LB} versus D keeping V_d constant	25
Figure 2-17	Discontinuous conduction in step-down converter	27
Figure 2-18	Step-down converter characteristics keeping V_d constant	28
Figure 2-19	Output voltage ripple in a step-down converter	29
Figure 2-20	Simple step down converter	30
Figure 2-21	PWM circuit used for stabilizing the output voltage	31
Figure 3-1	The circuit diagram used to determine I_s	35
Figure 3-2	The voltage cell as a function of the saturation current I_s	36
Figure 3-3	The circuit diagram used to determine R_s	37
Figure 3-4	The voltage cell as a function of internal resistance R_s	38
Figure 3-5	The electrical circuit of the model SP75	39
Figure 3-6	The output voltage panel $V(PV)$ as a function of the internal resistance R_s	40
Figure 3-7	The $(I - V)$ curve of the panel SP75 under TSC	41
Figure 3-8	The $(I - V)$ curve of the panel SP75 at different temperature under a constant irradiation $1000W/m^2$	43

Figure 3-9	The ($I - V$) curve of the panel SP75 at different irradianations under a constant temperature $T=25C^{\circ}$	44
Figure 3-10	The ($P - V$) curve of the panel SP75 under TSC	45
Figure 3-11	The ($P - V$) curve of the panel SP75 at different temperatures under a constant irradiation $1000W/m^2$	46
Figure 3-12	The ($P - V$) curve of the panel SP75 at different irradianations under a constant temperature $T = 25C^{\circ}$	47
Figure 3-13	The hierarchical block (part) of SP75 in state of (a) open circuit voltage condition. (b) optimum load condition	48
Figure 3-14	The ($I - V$) curve of the part SP75 at different temperatures under a constant irradiation $1000W/m^2$	49
Figure 3-15	The ($I - V$) curve of the part SP75 at different irradianations under a constant temperature $T = 25C^{\circ}$	50
Figure 3-16	The ($P - V$) curve of the part SP75 at different temperatures under a constant irradiation $1000W/m^2$	51
Figure 3-17	The ($P - V$) curve of the part SP75 at different irradianations under a constant temperature $T = 25C^{\circ}$	52
Figure 4-1	The step down converter configured in pspice	53
Figure 4-2	The complete system of the PWM generator	56
Figure 4-3	The gate drive circuit	57
Figure 4-4	The sources control circuit	58
Figure 4-5	The complete design of the two input PWM buck converter (interchange between the source operations)	60
Figure 4-6	The waveform patterns in boundary represent V_{out} , I_{out} in case of PV panel is on, $D=0.5$	61
Figure 4-7	The waveform patterns in boundary represent V_{out} , I_{out} in case of battery is on, $D=0.5$	61
Figure 4-8	The waveform patterns in boundary represent $V_{inductor}$, $I_{inductor}$ in case of PV panel is on, $D=0.5$	62
Figure 4-9	The waveform patterns in boundary represent $V_{inductor}$, $I_{inductor}$ in case of battery is on, $D=0.5$	62
Figure 4-10	The waveform patterns in boundary represent $V_{trigger}$, V_{pwm} in case of PV panel is on, $D=0.5$	63
Figure 4-11	The waveform patterns in boundary represent $V_{trigger}$, V_{pwm} in case of battery is on, $D=0.5$	63
Figure 4-12	The waveform patterns in discontinuous conduction mode for V_{out} , I_{out} in case of PV panel is on, $D < 0.5$	64
Figure 4-13	The waveform patterns in discontinuous conduction	64

	mode for V_{out} , I_{out} in case of the battery is on, $D < 0.5$	
Figure 4-14	The waveform patterns in discontinuous conduction mode for $V_{inductor}$, $I_{inductor}$ in case of PV panel is on, $D < 0.5$	65
Figure 4-15	The waveform patterns in discontinuous conduction mode for $V_{inductor}$, $I_{inductor}$ in case of the battery is on, $D < 0.5$	65
Figure 4-16	The waveform patterns in discontinuous conduction mode for $V_{trigger}$, V_{pwm} in case of PV panel is on, $D < 0.5$	66
Figure 4-17	The waveform patterns in discontinuous conduction mode for $V_{trigger}$, V_{pwm} in case of the battery is on, $D < 0.5$	66
Figure 4-18	The waveform patterns in continuous conduction mode for V_{out} , I_{out} in case of PV panel is on, $D > 0.5$	67
Figure 4-19	The waveform patterns in continuous conduction mode for V_{out} , I_{out} in case of the battery is on, $D > 0.5$	67
Figure 4-20	The waveform patterns in continuous conduction mode for $V_{inductor}$, $I_{inductor}$ in case of PV panel is on, $D > 0.5$	68
Figure 4-21	The waveform patterns in continuous conduction mode for $V_{inductor}$, $I_{inductor}$ in case of the battery is on, $D > 0.5$	68
Figure 4-22	The waveform patterns in continuous conduction mode for $V_{trigger}$, V_{pwm} in case of PV panel is on, $D > 0.5$	69
Figure 4-23	The waveform patterns in continuous conduction mode for $V_{trigger}$, V_{pwm} in case of the battery is on, $D > 0.5$	69

List of Symbols & Abbreviations

Is	saturation current
N	emission coefficient
Rs	parasitic resistance
XTI	Is temperature exponent
IKF	high-injection knee current
EG	bandgap voltage (barrier height)
Cjo	zero-bias p-n capacitance
M	p-n grading coefficient
VJ	p-n potential
Fc	forward-bias depletion capacitance coefficient
ISR	recombination current parameter
NR	emission coefficient for ISR
BV	reverse breakdown knee voltage
IBV	reverse breakdown knee current
Mpp	maximum power point
EMF	electromotive force in volt
VB	band potential difference in volt
τ	relaxation time in second
L	diffusion length
Ir	recombination current
Ig	generation current
ID	forward current passes through the p-n junction with no illumination
e	electron charge
V	potential appears on p-n junction
K	Boltezman constant
T	temperature in kalven
Vt	thermal voltage in volt
Voc	open circuit voltage of PV system
Isc	short circuit current of PV system
Vm	optimum voltage
Im	optimum current
η	efficiency
FF	Fill factor, A measure of the squareness of the largest rectangle area that can be fitted under the curve

I_L	light current
R_p	shunt resistance across the p-n junction
TSC	test standard conditions
P_{var}	solar irradiation in watt per square meter
R_s	series resistance of PV model in ohm
V_d	input voltage applied on DC-DC converter
t_{on}	on time of the control signal
T_s	switching time of the control signal
f_s	switching frequency of the control signal
D	duty cycle
V_o	output voltage of the DC-DC converter
L	inductance in μH
C	capacitance in μF
I_{LB}	average inductor current in boundary mode
i_L	ac inductor current
v_L	ac inductor voltage
PWM	pulse width modulation

List of tables

Table 2-1	Electric characteristics of the panel SP75 under TSC	21
-----------	--	----

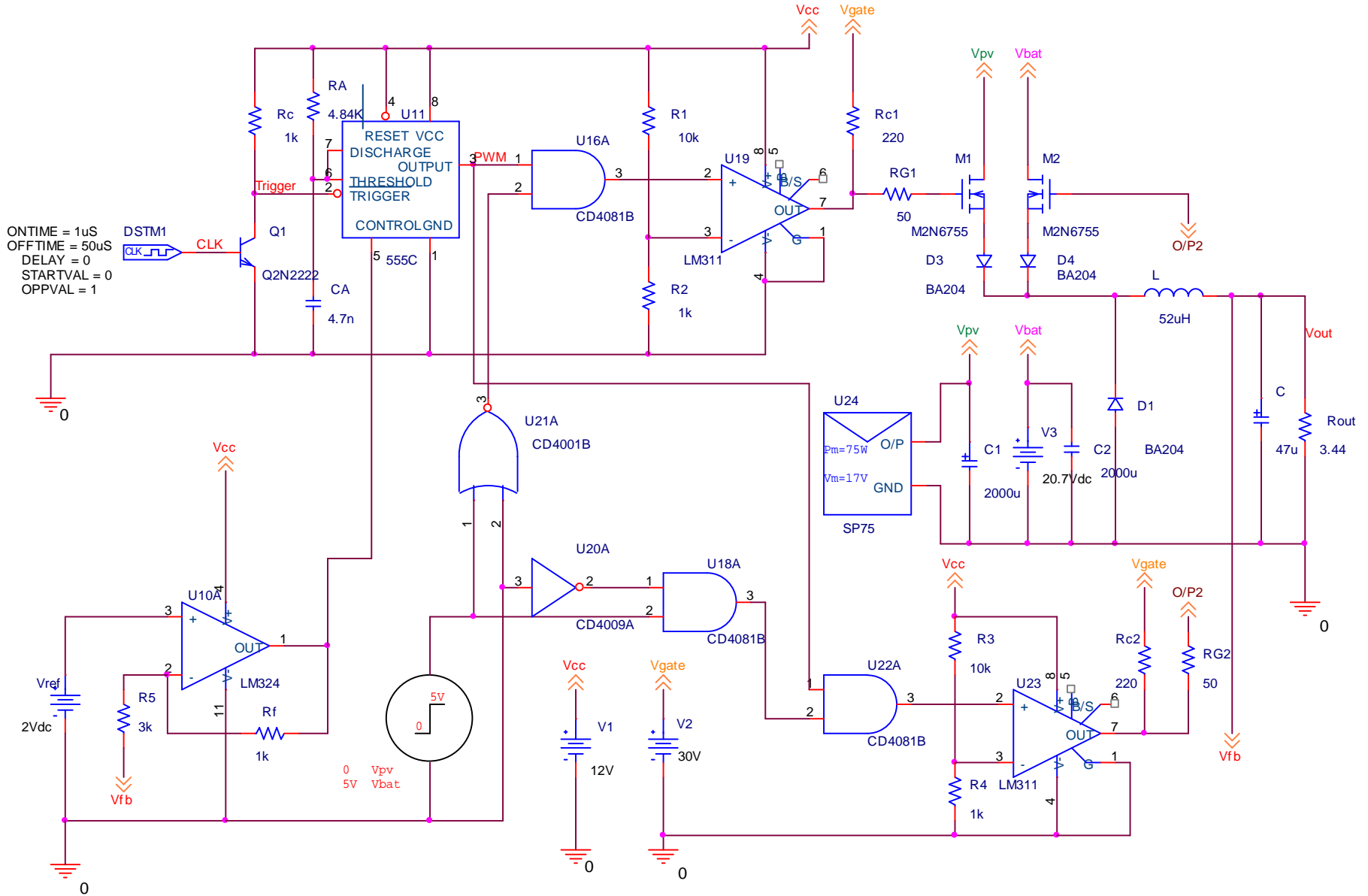


Figure 4-5: The complete design of the two input PWM buck converter (interchange between the source operations).